HERON is jointly edited by:
STEVIN-LABORATORY of the
faculty of Civil Engineering,
Delft University of Technology,
Delft, The Netherlands
and
TNO-INSTITUTE
FOR BUILDING MATERIALS
AND STRUCTURES.
Rijswijk (ZH), The Netherlands
HERON contains contributions
based mainly on research work
performed in these laboratories
on strength of materials, structures
and materials science.

ISSN 0046-7316

Secretary:
G. J. van Alphen
Stevinweg 1
P.O. Box 5048
2600 GA Delft, The Netherlands
Tel. 0031-15-785919
Telex 38070 BITHD

HERON vol. 34
1989
no. 1

Contents

CRACK MODELS FOR CONCRETE: DISCRETE OR SMEARED? FIXED, MULTI-DIRECTIONAL OR ROTATING?

J. G. Rots
Delft University of Technology,
Faculty of Civil Engineering/
TNO Institute for Building Materials and Structures,
Department of Computational Mechanics

J. Blaauwendraad
Delft University of Technology,
Faculty of Civil Engineering

This publication has been issued in close co-operation with the Netherlands Technology Foundation (STW).

Publication in HERON since 1970

Abstract

Numerical tools to simulate cracking in concrete and similar materials are developed. Firstly, a treatment is given of smeared and discrete crack concepts, which start from the notion of a continuum and a discontinuum respectively. With the smeared crack concept a distinction is furthermore made between fixed, multi-directional and rotating cracks, whereby the orientation of the crack is kept constant, updated in a stepwise manner or updated continuously respectively. Secondly, descriptions of the material behavior at cracking and fracture are presented. Key-effects herein are the tensile-softening behaviour normal to the crack (mode I) and the shear retention parallel to the crack (mode II). Thirdly, the resulting models are applied to scrutinize localized fracture in concrete. Attention is given to tension-shear problems whereby the principal stresses rotate after crack initiation, as is typical of general crack analysis. The results for the various crack concepts show large discrepancies. Smeared cracks may give rise to stress-locking while discrete cracks do not. Fixed smeared cracks may produce overstiff behavior while rotating smeared cracks do not.

1. Introduction

Tensile failure in matrix-aggregate composites like concrete involves progressive micro-cracking, tortuous debonding and other processes of internal damage. These softening processes eventually coalesce into a geometrical discontinuity that separates the material. Such a discontinuity is called a crack.

Undoubtedly, the discrete crack concept is the approach that reflects this phenomenon most closely. It models the crack directly via a displacement-discontinuity in an interface element that separates two solid elements. Unfortunately, the approach does not fit the nature of the finite element displacement method and it is computationally more convenient to employ a smeared crack concept. A smeared crack concept imagines the cracked solid to be a continuum and permits a description in terms of stress-strain relations. However, here the converse drawback occurs, since the underlying assumption of displacement continuity conflicts with the realism of a *dis*continuity.

To date, there is no consensus on the question which type of approach should be preferred. The confusion is even worse since the class of smeared crack concepts itself already offers a variety of possibilities, ranging from fixed single to fixed multi-directional and rotating crack approaches. Here, the distinction lies in the orientation of the smeared crack, which is either kept constant, updated in a stepwise manner or updated continuously. This confusion regarding crack concepts clearly appeared from, for example, the discussions during the IABSE Colloquium on Computational Mechanics of Concrete Structures at Delft in 1987.

It is the purpose of this article to investigate the merits and demerits of the various approaches. Recently, a few similar comparative studies have been presented, but these were mainly concerned with single-element problems of distributed fracture (e.g. Balakrishnan and Murray 1987, Willam et al. 1987, Barzegar 1989, Crisfield and Wills 1989). In the present article the focus is placed on localized fracture in element assemblies.

The outline of this article is as follows. Chapter 2 starts with an overview of crack concepts for numerical analysis. The treatment of the smeared crack approach is presented in a way that unifies the fixed single, multi-directional and rotating variants. Chapter 3 addresses material descriptions for concrete fracture. Particular forms of tension-softening and shear-retention functions are put forward for fixed single, multi-directional as well as rotating cracks. Chapter 4 compares the various models for an elementary tension-shear model problem and chapter 5 considers two tension-shear structural problems. These problems are designed such that the principal stress rotates beyond cracking, as is typical of general crack analysis. It is here that the discrepancies between the various concepts can be illustrated most clearly.

2. Crack concepts

Crack concepts can be categorized into discrete concepts and smeared concepts. The former approach models a crack as a geometrical discontinuity, whereas the latter imagines a cracked solid to be a continuum. This chapter reviews and develops both approaches with prime attention to the class of smeared crack concepts. The treatise is given in incremental form using matrix-vector notation, whereby we consider the general case of a three-dimensional configuration. Whenever stiffness moduli appear, their meaning will remain abstract since the correlation with the underlying material properties is postponed until the next chapter.

2.1 Discrete crack concept

In the early days of finite element analysis cracks were modeled by means of a separation between element edges (Ngo and Scordelis 1967, Nilson 1968). The approach suffers from two drawbacks. First, it implies a continuous change in nodal connectivity, which does not fit the nature of the finite element displacement method. Secondly, the crack is constrained to follow a predefined path along the element edges. The drawbacks are generally considered to be serious and attempts to eliminate them have been reported only sporadically. Prominent amongst these are the introduction of graphics-aided algorithms of automatic remeshing (Ingraffea and Saouma 1985) and of techniques which permit discrete cracks to extend through finite elements (Blaauwendraad and Grootenboer 1981, Blaauwendraad 1985).

A class of problems exists, however, whereby the orientation of the discrete crack is not necessarily the prime subject of interest. One may think of mode I fracture in the form of a straight separation band, the location of which is known in advance, or of discrete cracks along the interface between concrete and reinforcement. Furthermore, engineering problems exist whereby a mechanism of discrete cracks can be imagined to occur in a fashion similar to yield line mechanisms. For such cases, the above drawbacks vanish and one may use a simple form of discrete cracks with a predefined orientation.

In this study numerical experiments will be undertaken using a concept of predefined locations of potential cracking. To this end, interface elements are incorporated within the original mesh. The initial stiffness of the elements is assigned a large dummy value in order to simulate the uncracked state with rigid connection between overlapping nodes. Upon violating a condition of crack initiation, for instance a maximum stress condition, the element stiffness is changed and a constitutive model for discrete cracks is mobilized. Such a model links the tractions t^{cr} across the crack

to the relative displacements u^{cr} across the crack via C^{cr} which represents phenomena like tension-softening and aggregate interlock:

$$\Delta t^{cr} = C^{cr} \Delta u^{cr} \tag{2.1}$$

For a two-dimensional configuration the relative displacement vector consist of a mode I opening component and a mode-II sliding component, while a mode III sliding component is added in case of a third dimension. In a similar fashion, the traction vector comprises a mode I traction and mode-II and/or mode-III shear tractions.

Caution should be exercised in selecting the type of interface element. A distinction can be made between lumped interface elements (Ngo and Scordelis 1967) which evaluate the tractions and displacements at isolated node-sets, and continuous interface elements (Goodman et al. 1968) which smooth the behavior along an interpolated field. It has sometimes been suggested that the latter class of elements is superior. However, Rots (1988) and, independently, a number of researchers from geomechanics (e.g. Hohberg and Bachmann 1988) have found that this is not generally true. This relates to the question how large the dummy stiffness can and should be made. Ideally, it should be made extremely large to keep the initial dummy separation negligible. With the continuous interface elements such high stiffness values turn out to produce significant flutter in the traction profiles, whereas with the lumped interface elements the results for increasing dummy stiffness correctly converged towards the rigid-connection solution. In this paper we will therefore only employ the simple, lumped interface elements.

In this study the above approach has been pursued to perform comparative studies with smeared crack approaches. Other capabilities relate to the possibility of predefining the potential cracks not only at a limited number of locations, but anywhere in between the solid elements. The resulting configuration then corresponds to a set of elastic blocks bonded together by potential discrete cracks and the fracture is allowed to propagate anywhere in between the blocks. This approach resembles the distinct element method pioneered in geomechanics (Cundall and Strack 1979) and gaining popularity in fracture research (Roelfstra et al. 1985, Bazant 1986, Lorig and Cundall 1987).

2.2 Smeared crack concept

2.2.1 Essentials

The counterpart of the discrete crack concept is the smeared crack concept, in which a cracked solid is imagined to be a continuum. The approach, introduced by Rashid

(1968) starts from the notion of stress and strain and permits a description in terms of stress-strain relations. It is sufficient to switch from the initial isotropic stress-strain law to an orthotropic law upon crack formation, with the axes of orthotropy being determined according to a condition of crack initiation. The procedure is attractive not only because it preserves the topology of the original finite element mesh, but also because it does not impose restrictions with respect to the orientation of the crack planes, i.e. the axes of orthotropy. It is for these two reasons that the smeared concept quickly replaced the early discrete concepts and came into widespread use during the 1970s.

Ever since cracking has been modeled, the discrete concept and the smeared concept have been the subject of much controversy. The discrete concept fits our natural conception of fracture since we generally identify fracture as a true, geometrical discontinuity. Conversely, it has been stated that a smeared representation might be more realistic considering the "bands of micro-cracks" that blunt fracture in matrix-aggregate composites like concrete. The width of such bands, which occur at the tip of the visible crack, has even been claimed to be a material property (Bazant and Oh 1983). At present, however, it is difficult to judge these arguments since experimental detections of crack tip related micro-mechanical processes in matrix-aggregate composites are scarce and contradictory as far as the question is concerned whether these processes occur in a discrete manner or not (Diamond and Bentur 1985, Tait and Garret 1986). In this study the application of the smeared concept to cases of localized fracture is therefore considered to be an artifice for computational convenience.

The arguments change when we consider distributed fracture. Examples are the diffuse crack patterns in large-scale shear walls or panels due to the presence of densely distributed reinforcement. Such cases provide a true physical basis for smeared concepts, at least if the scale of the representative continuum is large compared to the crack spacing. Even stronger, the smeared concept seems to be the only rational approach towards distributed fracture since the use of a discrete concept, which considers each individual crack as though "under a magnifying glass" then becomes clearly unwieldy. This article will not touch on distributed fracture.

Smeared crack concepts can be categorized into fixed and rotating smeared crack concepts. With a fixed concept the orientation of the crack is fixed during the entire computational process, whereas a rotating concept allows the orientation of the crack to co-rotate with the axes of principal strain. This section addresses these two classes of concepts as well as the intermediate option of a fixed multi-directional smeared crack concept. Recent routes of modeling smeared cracks within the framework of plasticity (Willam et al. 1987, Crisfield and Wills 1989, Lubliner et al. 1989) are left out of consideration.

2.2.2 Standard fixed smeared crack concept

Traditionally, the stress-strain law for smeared cracking has been set-up with reference to fixed principal n,s,t-axes of orthotropy, where n refers to the direction normal to the crack (mode I) and s,t refer to the directions tangential to the crack (mode II and mode-III),

$$\begin{bmatrix} \sigma_{nn} \\ \sigma_{ss} \\ \sigma_{tt} \\ \sigma_{ns} \\ \sigma_{st} \\ \sigma_{tn} \end{bmatrix} = \begin{bmatrix} E_{nn} & E_{ns} & E_{nt} & 0 & 0 & 0 \\ E_{ns} & E_{ss} & E_{st} & 0 & 0 & 0 \\ E_{nt} & E_{st} & E_{tt} & 0 & 0 & 0 \\ 0 & 0 & 0 & G_{ns} & 0 & 0 \\ 0 & 0 & 0 & 0 & G_{st} & 0 \\ 0 & 0 & 0 & 0 & 0 & G_{nt} \end{bmatrix} \begin{bmatrix} \varepsilon_{nn} \\ \varepsilon_{ss} \\ \varepsilon_{tt} \\ \gamma_{ns} \\ \gamma_{st} \\ \gamma_{tn} \end{bmatrix} \tag{2.2}$$

which is defined by nine independent stiffness moduli.

In the earliest versions (Rashid 1968, Cervenka 1970, Valliappan and Doolan 1972) E_{nn}, E_{ns}, E_{nt}, G_{ns} and G_{nt} were set equal to zero, involving the crack normal stress σ_{nn} and the crack shear stresses σ_{ns} and σ_{tn} to abruptly drop to zero upon crack formation. This is a crude approximation of reality as cracks in heterogeneous materials may well be capable of transmitting tension stresses in mode I and shear stresses in mode-II due to tortuous debonding and interlock. Moreover, the sudden switch from the initial isotropic linearly-elastic law to an orthotropic law with zero stiffness moduli implies a strong discontinuity which turned out to amplify numerical difficulties (Schnobrich 1972). For these reasons, researchers reinserted the initial isotropic stiffness moduli with some percentage of reduction. For instance, Suidan and Schnobrich (1973) reinserted G_{ns} and G_{nt} as a percentage of the initial linear-elastic shear modulus G. The corresponding reduction factor was called the shear stiffness reduction or shear retention factor β. Bazant and Oh (1983) broadened the concept by reinserting the stiffness E_{nn} normal to the crack as a percentage of the initial Young's modulus E, whereby they also introduced non-zero off-diagonal stiffness moduli so as to incorporate Poisson's effect after cracking. In the 1980s the following incremental relation evolved into a popular orthotropic law for a two-dimensional configuration (e.g. Leibengood et al. 1986, Rots et al. 1984):

$$\begin{bmatrix} \Delta\sigma_{nn} \\ \Delta\sigma_{tt} \\ \Delta\sigma_{nt} \end{bmatrix} = \begin{bmatrix} \dfrac{\mu E}{1-\nu^2\mu} & \dfrac{\nu\mu E}{1-\nu^2\mu} & 0 \\ \dfrac{\nu\mu E}{1-\nu^2\mu} & \dfrac{E}{1-\nu^2\mu} & 0 \\ 0 & 0 & \dfrac{\beta E}{2(1+\nu)} \end{bmatrix} \begin{bmatrix} \Delta\varepsilon_{nn} \\ \Delta\varepsilon_{tt} \\ \Delta\gamma_{nt} \end{bmatrix} \tag{2.3}$$

E is Young's modulus, ν is Poisson's ratio, μ is the reduction factor for the mode I stiffness which is negative in case of softening, and β is the shear retention factor.

2.2.3 Fixed smeared crack concept with strain-decomposition

The strain-vectors in (2.2) and (2.3) represent an overall strain of the cracked solid, which includes the strain due to cracking as well as the strain of the solid material between the cracks. The resulting stress-strain laws correspond to a smeared-out relation for the cracked solid, without making any distinction between the cracks and the solid material in between the cracks. The disadvantage is that particular crack laws, which start from the notion of crack strain rather than total strain, can not be incorporated in a transparent manner. Indeed, a gap tended to develop between the sophisticated crack models developed by materials scientists and the coarse smeared crack concepts employed by structural analysts. For instance, the choice of the shear retention factor was often made arbitrarily without reference to aggregate-interlock models.

A solution to this deficiency is to decompose the total strain $\Delta\varepsilon$ of the cracked material into a part $\Delta\varepsilon^{cr}$ of the crack and a part $\Delta\varepsilon^{co}$ of the solid material (superscript *co* of concrete) between the cracks,

$$\Delta\varepsilon = \Delta\varepsilon^{cr} + \Delta\varepsilon^{co} \tag{2.4}$$

The importance of the decomposition has been recognized by a number of researchers (Litton 1974, Bazant and Gambarova 1980, de Borst and Nauta 1985, Rots et al. 1985, Riggs and Powell 1986). It is in essence an attempt to come closer to the discrete crack concept which completely separates the solid material from the crack by using separate finite elements.

The strain vectors in (2.4) relate to the global coordinate axes and for a three-dimensional configuration they have six components. The global crack strain vector reads

$$\Delta\varepsilon^{cr} = \left[\Delta\varepsilon_{xx}^{cr}\ \Delta\varepsilon_{yy}^{cr}\ \Delta\varepsilon_{zz}^{cr}\ \Delta\gamma_{xy}^{cr}\ \Delta\gamma_{yz}^{cr}\ \Delta\gamma_{zx}^{cr} \right]^T \tag{2.5}$$

where x,y and z refer to the global coordinate axes and the superscript T denotes a transpose. When incorporating crack traction-crack strain laws it is convenient to set up a local n,s,t-coordinate system which is aligned with the crack, as shown in Fig. 2.1. In the local system, we define a local crack strain vector Δe^{cr},

$$\Delta e^{cr} = \left[\Delta\varepsilon_{nn}^{cr} \;\; \Delta\gamma_{ns}^{cr} \;\; \Delta\gamma_{nt}^{cr} \right]^T \tag{2.6}$$

where ε_{nn}^{cr} is the mode I crack normal strain and γ_{ns}^{cr}, γ_{nt}^{cr} are the mode II and mode III crack shear strains respectively. The three remaining crack strain components in the local system do not have a physical meaning and can be omitted.

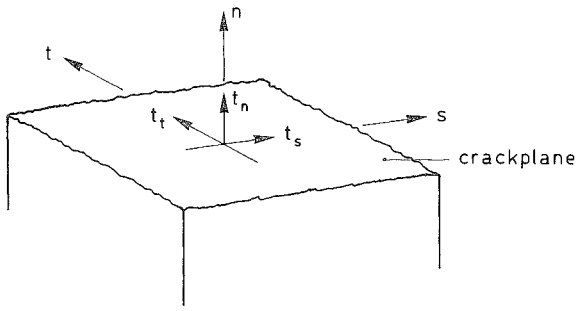

Fig. 2.1. Local coordinate system and tractions across a crack.

The relation between local and global crack strains reads

$$\Delta\varepsilon^{cr} = N\Delta e^{cr} \tag{2.7}$$

with N being a transformation matrix reflecting the orientation of the crack. A fundamental feature of the present concept is that N is assumed to be *fixed* upon crack formation, so that the concept belongs to the class of fixed crack concepts. For a three-dimensional configuration N reads

$$N = \begin{bmatrix} l_x^2 & l_x l_y & l_z l_x \\ m_x^2 & m_x m_y & m_z m_x \\ n_x^2 & n_x n_y & n_z n_x \\ 2l_x m_x & l_x m_y + l_y m_x & l_z m_x + l_x m_z \\ 2m_x n_x & m_x n_y + m_y n_x & m_z n_x + m_x n_z \\ 2n_x l_x & n_x l_y + n_y l_x & n_z l_x + n_x l_z \end{bmatrix} \tag{2.8}$$

where l_x, m_x and n_x form a vector which indicates the direction of the local n-axis expressed in the global coordinates. In accordance with this convention, the direction cosines with subscript y indicate the local s-axis and those with subscript z indicate the local t-axis. For a plane-stress configuration the third column and the third, fifth and sixth row of (2.8) vanish, rendering a 3*2 matrix, while for axi-symmetric and plane-

strain configurations the third column and the fifth and sixth row of (2.8) vanish, rendering a 4*2 matrix. Here, the reduced number of rows corresponds to the reduced number of global strain components, while the reduction from three to two columns arises from the fact that the mode III component vanishes.

In the local coordinate system, we define a vector Δt^{cr} of incremental tractions across the crack

$$\Delta t^{cr} = \left[\Delta t_n^{cr} \; \Delta t_s^{cr} \; \Delta t_t^{cr} \right]^T \tag{2.9}$$

in which Δt_n^{cr} is the mode I normal traction and Δt_s^{cr}, Δt_t^{cr} are mode II and mode III shear traction increments, as shown in Fig. 2.1. The relation between the global stress increment $\Delta\sigma$ and the local traction increment can be derived to be

$$\Delta t^{cr} = N^T \Delta\sigma \tag{2.10}$$

To complete the system of equations, we need a constitutive model for the intact concrete and a traction-strain relation for the smeared cracks. For the concrete between the cracks a relationship is assumed of the following structure

$$\Delta\sigma = D^{co} \Delta\varepsilon^{co} \tag{2.11}$$

with the matrix D^{co} containing the instantaneous moduli of the concrete. In a similar way, a relation is inserted between the local crack strain and the local tractions,

$$\Delta t^{cr} = D^{cr} \Delta e^{cr} \tag{2.12}$$

with D^{cr} a 3*3 matrix incorporating the mode I, mode II, mode-III and mixed-mode properties of the crack.

By properly combining Eqs. (2.4), (2.7), (2.10), (2.11) and (2.12) the overall stress-strain relation for the cracked concrete with respect to the global coordinate system can be developed. To this end, (2.7) is substituted into (2.4), and subsequently (2.4) into (2.11), which yields

$$\Delta\sigma = D^{co}[\Delta\varepsilon - N\Delta e^{cr}] \tag{2.13}$$

Pre-multiplying (2.13) by N^T and substituting (2.12) and (2.10) into the resulting left side of (2.13) yields the link between local crack strain and global strain,

$$\Delta e^{cr} = [D^{cr} + N^T D^{co} N]^{-1} N^T D^{co} \Delta\varepsilon \tag{2.14}$$

Finally, the overall relation between global stress and global strain is obtained by substituting (2.14) into (2.13),

$$\Delta\sigma = [D^{co} - D^{co}N[D^{cr} + N^T D^{co} N]^{-1} N^T D^{co}]\Delta\varepsilon \tag{2.15}$$

The expression between the outer brackets will be referred to as D^{crco} in the sequel (superscript crco of cracked concrete).

The incremental formulation of the concept entails two complications. First, (2.15) implies a linearization around the current state, which means that the stress increment computed holds exactly only if D^{co} as well as D^{cr} remain constant during the current strain increment. If either of these matrices is non-constant, which for instance occurs if the concrete model involves plasticity or if the crack model involves nonlinear fracture functions, (2.15) only serves as a first order approximation. A corrective procedure then becomes necessary in order to circumvent drifting from either the concrete or the crack stress-strain law. This study considers the case of nonlinear fracture functions, i.e. nonlinearity in D^{cr}. A possible corrective procedure is then provided by an inner iteration loop that repeatedly evaluates (2.14) and (2.12), starting from a predictor using tangent crack stiffness moduli and proceeding by correctors using secant crack stiffness moduli, as detailed before (Rots 1986). Such a forward-Euler scheme performed adequately with the examples considered in this thesis. However, in case of strong discontinuities (e.g. very steep softening) the method may sometimes fail and extensions along the line of sub-increments or other techniques are required that accommodate a more rigorous return to the fracture functions.

Secondly, an incremental simulation involves the state of the solid to be subject to change, owing to initiation, closing and re-opening of cracks. To handle state changes we employ a procedure that subdivides the strain path. When the criteria of initiation, closing and re-opening indicate a change of state during the current load increment, the total strain increment $\Delta\varepsilon$ is split into a pre-transition part $\Delta\varepsilon^a$ and a post-transition part $\Delta\varepsilon^b$,

$$\Delta\varepsilon = \Delta\varepsilon^a + \Delta\varepsilon^b \tag{2.16}$$

The stress increment is subsequently computed from different stress-strain relations for the pre- and post-transition parts respectively. In this way, the transition from the uncracked state to the cracked state, which occurs when a new crack initiates or when a closed crack re-opens, gives

$$\Delta\sigma = D^{co}\Delta\varepsilon^a + D^{crco}\Delta\varepsilon^b \tag{2.17}$$

whereas the transition from the cracked state to the uncracked state, which occurs when a crack closes, gives

$$\Delta\sigma = D^{crco}\Delta\varepsilon^{a} + D^{co}\Delta\varepsilon^{b} \tag{2.18}$$

Locating the state transition point is a straightforward operation when D^{co} and D^{cr} are constants. If they are not, an inner iteration loop should be invoked to scale $\Delta\varepsilon^{a}$, so as to satisfy the initiation, closing or re-opening conditions with reasonable accuracy.

Criteria of closing and re-opening are generally defined in terms of total local crack stress or total local crack strain. As the fixed crack concept assumes the local crack axes to remain unaltered, these quantities are readily available in the form of an accumulation of previous increments. This *permanent memory of damage orientation* is the prominent feature of fixed smeared crack concepts.

2.2.4 Multi-directional fixed smeared crack concept

A further advantage of the decomposition of total strain into concrete strain and crack strain is that it allows for a sub-decomposition of concrete strain and crack strain on their turn. A sub-decomposition of the concrete strain (de Borst 1986) will not be considered here, but we will concentrate on a sub-decomposition of the crack strain into the separate contributions from a number of multi-directional cracks that simultaneously occur at a sampling point, i.e.

$$\Delta\varepsilon^{cr} = \Delta\varepsilon_1^{cr} + \Delta\varepsilon_2^{cr} + \ldots\ldots\ldots \tag{2.19}$$

where $\Delta\varepsilon_1^{cr}$ is the global crack strain increment owing to a primary crack, $\Delta\varepsilon_2^{cr}$ is the global crack strain increment owing to a secondary crack and so on.

The idea of a sub-decomposition of the crack strain was advocated by Litton (1974), de Borst and Nauta (1985) and Riggs and Powell (1986). The essence of their approach is that each (fixed) crack is assigned its own local crack strain vector e_i^{cr}, its own traction vector t_i^{cr} and its own transformation matrix N_i according to (2.6), (2.9) and (2.8) respectively. They furthermore demonstrated that it is convenient to assemble these single-crack vectors and matrices into

$$\Delta\hat{e}^{cr} = \left[\Delta e_1^{cr}\ \Delta e_2^{cr}\ \ldots\ldots\ldots\right]^{T} \tag{2.20}$$

$$\Delta\hat{t}^{cr} = \left[\Delta t_1^{cr}\ \Delta t_2^{cr}\ \ldots\ldots\ldots\right]^{T} \tag{2.21}$$

$$\hat{N} = \left[N_1\ N_2\ \ldots\ldots\ldots\right] \tag{2.22}$$

in which $\hat{}$ denotes an assembly of multi-directional cracks. Repeated substitution of (2.7) into (2.19) yields

$$\Delta\varepsilon^{cr} = \hat{N}\Delta\hat{e}^{cr} \tag{2.23}$$

which is the multiple-crack equivalent of (2.7). In a similar way, the single-crack traction-strain relations can be expanded into a multiple-crack equivalent of (2.12),

$$\Delta\hat{t}^{cr} = \hat{D}^{cr}\Delta\hat{e}^{cr} \tag{2.24}$$

or, in the elaborated form,

$$\begin{bmatrix} \Delta t_1^{cr} \\ \Delta t_2^{cr} \\ \cdots\cdots \end{bmatrix} = \begin{bmatrix} D_{11}^{cr} & D_{12}^{cr} & \cdots\cdots \\ D_{21}^{cr} & D_{22}^{cr} & \cdots\cdots \\ \cdots\cdots & \cdots\cdots & \cdots\cdots \end{bmatrix} \begin{bmatrix} \Delta e_1^{cr} \\ \Delta e_2^{cr} \\ \cdots\cdots \end{bmatrix}$$

which is a very general relation since it allows for interaction between the cracks via the off-diagonal submatrices.

Repeating the procedure of the previous section, we end up with the analogy of (2.15) for multi-directionally cracked concrete:

$$\Delta\sigma = [D^{co} - D^{co}\hat{N}[\hat{D}^{cr} + \hat{N}^T D^{co}\hat{N}]^{-1}\hat{N}^T D^{co}]\Delta\varepsilon \tag{2.25}$$

The assembled matrices $\hat{N}$ and $\hat{D}^{cr}$ are inserted instead of the single-crack matrices N and D^{cr}.

Considering sampling points with multi-directional cracks, the issue of state changes becomes increasingly pressing and sometimes even failure of the implementation was reported for this reason (Crisfield and Wills 1989). In the present study, the procedure of transition points, as outlined in the preceding for single cracks, has been unambiguously extended to include state changes for multi-directional cracks. Considering a current configuration of i unclosed cracks, and dividing the strain-increment $\Delta\varepsilon$ into a pre-transition part $\Delta\varepsilon^a$ and a post-transition part $\Delta\varepsilon^b$, the state change due to initiation of a new crack or re-opening of a closed crack gives

$$\Delta\sigma = \hat{D}_i^{crco}\Delta\varepsilon^a + \hat{D}_{i+1}^{crco}\Delta\varepsilon^b \tag{2.26}$$

whereas the state change due to closing of one of the cracks gives

$$\Delta\sigma = \hat{D}_i^{crco}\Delta\varepsilon^a + \hat{D}_{i-1}^{crco}\Delta\varepsilon^b \tag{2.27}$$

where $\hat{D}_{i-1}^{crco}$, $\hat{D}_{i}^{crco}$ and $\hat{D}_{i+1}^{crco}$ denote the overall stress-strain matrices of (2.25) for configurations of $i-1$, i and $i+1$ unclosed cracks respectively, which are based on the underlying assembled local traction-strain matrices $\hat{D}_{i-1}^{cr}$, $\hat{D}_{i}^{cr}$ and $\hat{D}_{i+1}^{cr}$ of (2.24) and on the underlying assembled transformation matrices $\hat{N}_{i-1}$, $\hat{N}_{i}$ and $\hat{N}_{i+1}$ of (2.22). Consequently, whenever a new crack initiates or a closed crack re-opens $\hat{D}^{cr}$ and $\hat{N}$ are expanded to include the associated submatrices, while they are compressed on crack closure to delete the associated submatrices. The magnitude of the pre-transition strain increment $\Delta\varepsilon^a$ must be scaled so as to satisfy the initiation, closing or re-opening condition with reasonable accuracy.

A state change for one of the cracks promotes state changes of the others. For instance, the initiation of a new crack encourages existing cracks to close. If such multiple state changes occur during the current strain increment, the "most critical" state change should be traced and handled first, while subsequent state changes should be treated by splitting $\Delta\varepsilon^b$ on its turn. Depending on the particular crack closing condition, this procedure may become elusive and it may be more convenient to allow only one crack to change its state, while possible state changes of other cracks are postponed until the next stage of the incremental simulation. In the latter case, inconsistencies cannot entirely be avoided, since postponing crack closing involves the crack normal strain to temporarily become negative, which is physically meaningless.

The significance of the multi-directional crack concept is obvious in conditions of biaxial or triaxial tension. Here, we expect two or three *orthogonal* cracks, the behavior of each of which can be monitored separately keeping record of memory. This option is particularly relevant with axi-symmetric and plane-strain analysis, where numerous points may be cracked longitudinally as well as transversely.

A second important field of application is given by conditions of tension-shear, which is typical of fracture propagation problems with the fracture starting in tension (mode I) and subsequently proceeding in tension-shear (mixed-mode). This behavior implies that the axes of principal stress rotate after crack formation, which leads to an increasing discrepancy between the axes of principal stress and the fixed crack axes. Pending the treatment of the rotating crack concept, which rigorously eliminates the phenomenon by enforcing coaxiality between principal axes and crack axes, it is noted that the fixed multi-directional crack concept provides an alternative. Whenever the angle of inclination between the existing crack(s) and the current direction of principal stress exceeds the value of a certain *threshold angle*, a new crack is initiated. In this way, we end up with a system of *non-orthogonal* cracks as pioneered by de Borst and Nauta (1985).

2.2.5 Rotating smeared crack concept

The misalignment of principal directions and crack directions, as adhering to fixed crack concepts, prompted Cope et al. (1980) to co-rotate the axes of material orthotropy with the axes of principal strain. The approach subsequently evolved into the rotating crack concept. The concept is attractive from an engineering point of view, since the analyst can suffice to specifying non-linear stress-strain curves for the principal directions, without having to resort to abstract theories.

Bazant (1983) raised a number of objections to the earliest versions of the concept. One of them relates to the fact that the assumption of material orthotropy generally implies the rotation of principal stress to deviate from the rotation of principal strain. Consequently, when the axes of material orthotropy co-rotate with the axes of principal strain, they will cease to coincide with the axes of principal stress. The direct use of principal stress-strain curves then becomes inconsistent, unless transformation rules are included in the derivation of the tangential stiffness moduli.

Although he did not pursue this issue further, Bazant (1983) also outlined an important condition that enforces coaxiality between principal stress and strain. To illustrate this, consider a 2D configuration of initial coaxiality, with the principal 1,2 directions of stress, strain and material orthotropy being aligned. By virtue of Mohr's strain circle, a small increment of shear strain causes the direction of principal strain to rotate by an angle $\Delta\theta_\varepsilon$ according to

$$\tan 2\Delta\theta_\varepsilon = \frac{\Delta\gamma_{12}}{2(\varepsilon_{11}-\varepsilon_{22})} \tag{2.28}$$

if $|\Delta\gamma_{12}| \ll |\varepsilon_{11}-\varepsilon_{22}|$. Here, $\Delta\gamma_{12}$ is the shear strain increment in the 1,2 reference frame and $\varepsilon_{11}, \varepsilon_{22}$ are the initial principal strains. In a similar fashion, Mohr's stress circle indicates that a small increment of shear stress causes a principal stress rotation by an angle $\Delta\theta_\sigma$ according to

$$\tan 2\Delta\theta_\sigma = \frac{\Delta\sigma_{12}}{(\sigma_{11}-\sigma_{22})} \tag{2.29}$$

if $|\Delta\sigma_{12}| \ll |\sigma_{11}-\sigma_{22}|$. Preserving coaxiality between principal stress and strain requires $\Delta\theta_\varepsilon=\Delta\theta_\sigma$. Using the orthotropic law of (2.2) in the principal 1,2 reference frame, we observe that this condition is satisfied if and only if the tangential shear modulus G_{12} is given by

$$G_{12} = \frac{(\sigma_{11}-\sigma_{22})}{2(\varepsilon_{11}-\varepsilon_{22})} \tag{2.30}$$

The linearized form of the tangential stress-strain law for a consistent rotating crack concept then becomes

$$\begin{bmatrix} \Delta\sigma_{11} \\ \Delta\sigma_{22} \\ \Delta\sigma_{33} \\ \Delta\sigma_{12} \\ \Delta\sigma_{23} \\ \Delta\sigma_{31} \end{bmatrix} = \begin{bmatrix} \frac{\partial\sigma_{11}}{\partial\varepsilon_{11}} & \frac{\partial\sigma_{11}}{\partial\varepsilon_{22}} & \frac{\partial\sigma_{11}}{\partial\varepsilon_{33}} & 0 & 0 & 0 \\ \frac{\partial\sigma_{22}}{\partial\varepsilon_{11}} & \frac{\partial\sigma_{22}}{\partial\varepsilon_{22}} & \frac{\partial\sigma_{22}}{\partial\varepsilon_{33}} & 0 & 0 & 0 \\ \frac{\partial\sigma_{33}}{\partial\varepsilon_{11}} & \frac{\partial\sigma_{33}}{\partial\varepsilon_{33}} & \frac{\partial\sigma_{33}}{\partial\varepsilon_{33}} & 0 & 0 & 0 \\ 0 & 0 & 0 & \frac{\sigma_{11}-\sigma_{22}}{2(\varepsilon_{11}-\varepsilon_{22})} & 0 & 0 \\ 0 & 0 & 0 & 0 & \frac{\sigma_{22}-\sigma_{33}}{2(\varepsilon_{22}-\varepsilon_{33})} & 0 \\ 0 & 0 & 0 & 0 & 0 & \frac{\sigma_{33}-\sigma_{11}}{2(\varepsilon_{33}-\varepsilon_{11})} \end{bmatrix} \begin{bmatrix} \Delta\varepsilon_{11} \\ \Delta\varepsilon_{22} \\ \Delta\varepsilon_{33} \\ \Delta\gamma_{12} \\ \Delta\gamma_{23} \\ \Delta\gamma_{31} \end{bmatrix} \tag{2.31}$$

where the derivatives $\partial\sigma_{11}/\partial\varepsilon_{11}$ etc. can be inserted directly since the shear terms guarantee coaxiality between principal stress and strain.

Eq. (2.31) was developed in a more elegant way by Willam et al. (1987). An alternative formulation was derived by Gupta and Akbar (1984) and Crisfield and Wills (1989) who started from a description in a fixed x,y coordinate system.

It is intriguing to examine the parallels between the fixed multi-directional crack concept and the rotating crack concept. While the fixed multi-directional concept controls the formation of subsequent cracks via the threshold angle, the rotating concept assumes the crack orientation to change continuously. Assuming the threshold angle for multi-directional cracks to vanish, a new fixed crack arises at the beginning of each stage of the incremental process. In doing so, we observe that the fixed multi-directional concept reduces to the rotating concept, provided that

— the condition of a vanishing threshold angle is the *only* condition that controls the orientation of subsequent cracks, i.e. it is not augmented by a maximum stress condition as was done in a previous study (de Borst and Nauta 1985),

— previous cracks are rigorously made inactive and erased from memory upon activation of the new crack, so that we invariably have only one active crack

which is unique to the loading phase,

— the local traction-strain law (2.12) of the active crack is filled in such a way that (a) the memory of previous defects is accounted for, (b) the overall shear modulus ensures coaxiality according to (2.30).

In the present study, rotating cracks will be conceived in this fashion. The three listed conditions will be elaborated in section 3.3. Strictly speaking, the term 'rotating crack' no longer applies since we consider a collection of fixed tiny defects of different orientation, each of them having its own local traction-strain law, rather than a single rotating crack with a rotating principal stress-strain relation. As an advantage, a second objection against rotating crack concepts raised by Bazant (1983) namely that rotating defects against the material is unacceptable from a physical point of view, no longer applies either. Besides, with distributed fracture the notion of fixed defects of gradually rotating orientation is supported by experimental evidence (Vecchio and Collins 1986, Bhide and Collins 1987, Kolleger and Mehlhorn 1987). With localized fracture such experimental justification does not seem to exist, but there is little argument that mixed-mode crack tip processes involve fixed defects of gradually rotating orientation.

A further advantage of conceiving the rotating crack approach as the limiting case of the fixed multi-directional crack approach is that it maintains decomposition of total strain into concrete strain and crack strain. This permits the concrete material law (e.g. elasticity) to be satisfied exactly. With other versions of the rotating crack concept this is not necessarily true as these models generally lose Poisson's effect after cracking (Gupta and Akbar 1984, Milford and Schnobrich 1984, Balakrishnan and Murray 1987, Crisfield and Wills 1989). The strain-decomposition is also essential for a consistent combination of smeared cracking with plasticity, creep and thermal loading (de Borst 1987).

Since (2.31) is given in incremental form, a corrective procedure must be added in order to suppress drifting from the coaxiality condition as induced by evaluating (2.31) for finite increments of strain. To this purpose an inner iteration loop has been employed, whereby (2.31) is repeatedly evaluated using the initial tangential shear term $(\sigma^0_{11}-\sigma^0_{22})/2(\varepsilon^0_{11}-\varepsilon^0_{22})$ in the first inner iteration (predictor) and updated tangential shear terms $(\sigma^i_{11}-\sigma^i_{22})/2(\varepsilon^i_{11}-\varepsilon^i_{22})$ in subsequent iterations (correctors). Here, the superscript ^{0} refers to the initial state which is coaxial (except for previous inaccuracies), and ^{i} refers to the calculated state from the previous iteration. The procedure replicates the treatment of nonlinear fracture functions (Rots 1986) and shows fast convergence provided that the load increments are taken sufficiently small to prevent the stresses from rotating heavily. For the example problems in this thesis, a coaxiality norm of 0.1 degrees was easily achieved within less than five inner iterations.

The rotating crack concept differs from the fixed crack concepts in that it does not preserve permanent memory of the damage orientation. This implies that with the rotating crack concept inactive defects cannot be re-activated during a subsequent stage of the loading process, which has consequences when the loading process is non-proportional.

A second difference relates to the possibility of incorporating shear effects from e.g. aggregate interlock models. The fixed crack concepts fit the nature of such models since these also refer to a fixed crack plane. On the one hand, this is an advantage. On the other hand, the use of any crack shear relation for fixed cracks complicates the analysis because it is responsible for an often uncontrollable rotation of the axes of principal stress, which cease to coincide with the axes of principal strain. With the rotating crack concept these considerations hold in a converse manner. This concept accommodates a unique shear term that enforces coaxiality between principal stress and strain, which introduces simplicity, but it inherently abandons the possibility of incorporating different crack shear models since the crack always occurs in a principal direction, i.e. in mode I.

3. Elastic-softening material description

Having treated the crack concepts, the present chapter proceeds with embedding material descriptions into the concepts. For tension and tension-shear dominated problems an adequate model is constructed by assuming elasticity for the concrete and softening for the crack. The objective is to present a rational formulation of the softening component for fixed single, fixed multi-directional and rotating cracks successively.

3.1 Single-crack parameters

3.1.1 Essentials

Prior to cracking, concrete is represented sufficiently accurately as an isotropic, linear-elastic material. The parameters are Young's modulus E and Poisson's ratio ν. Upon crack initiation, the strain decomposition according to (2.4) is mobilized and for the concrete we continue with linear elasticity, while (2.1) or (2.12) is inserted for the crack. Eq. (2.1) relates the traction increment Δt^{cr} to the crack displacement increment Δu^{cr} for discrete cracks via C^{cr}, whereas (2.12) relates the traction increment to the crack strain increment Δe^{cr} for smeared cracks via D^{cr}. In the present study, these matrices are assumed to be of the form:

$$C^{cr} = \begin{bmatrix} C^I & 0 & 0 \\ 0 & C^{II} & 0 \\ 0 & 0 & C^{III} \end{bmatrix} \tag{3.1}$$

and

$$D^{cr} = \begin{bmatrix} D^I & 0 & 0 \\ 0 & D^{II} & 0 \\ 0 & 0 & D^{III} \end{bmatrix} \tag{3.2}$$

where C^I, C^{II}, C^{III} and D^I, D^{II}, D^{III} are the mode I, mode II and mode III stiffness moduli for a discrete single crack and a smeared single crack respectively.

The assumption of zero off-diagonal terms in (3.1) and (3.2) implies that direct shear-normal coupling has been ignored. This assumption arises from three considerations:

— To date, experimental evidence for the importance of coupling terms exists only for the case of confined sliding along macro-cracks. In that field, crack dilatancy theories with non-symmetric matrices have been proposed (Walraven 1980, Bazant and Gambarova 1980). In the present study the focus is placed on initiation and propagation of the crack rather than on sliding along an existing crack. For such cases, experimental data on direct shear-normal coupling are currently being produced (van Mier and Nooru-Mohamed 1988, Hassanzadeh and Hillerborg 1988), but were not yet available at the time of this study.

— Although (3.1) and (3.2) ignore direct shear-normal coupling, this effect may be obtained indirectly, by
  (a) allowing cracks to rotate, or allowing subsequent non-orthogonal cracks to form,
  (b) relating the diagonal terms of C^{cr} and D^{cr} not only to their associated displacement and strain component respectively, but also to the others (for instance, the shear modulus D^{II} can be made a function of the crack normal strain).

— It is instructive to start from simple models and to a posteriori discuss whether the simplifications are justified, or whether more complicated models are required. This discussion is provided by the next chapter and will highlight the technique of indirect coupling via non-orthogonal cracks.

A salient feature of the model components presented in the sequel is that they assume fracture to be initiated in mode I, whereas mode II or mode III shear effects

only enter upon subsequent rotation of the principal stresses. This hypothesis is supported by experimental evidence with respect to static loading conditions of tension and tension-shear (e.g. Arrea and Ingraffea 1982, Kobayashi et al. 1985, Jenq and Shah 1988). Contrary experimental results have been reported only for dynamic loadings (Harmsma and Nijhout 1982) and for very particular static loadings with a high mode II (Bazant and Pfeiffer 1986) or mode III (Bazant and Prat 1988) intensity. Such cases are beyond the scope of the present study.

The feature implies that distinction between mode II and mode III becomes irrelevant, so that notation will be confined to mode II.

3.1.2 Mode I parameters

Traditionally, a set of strength parameters has been introduced to control fracture initiation. These parameters locate a tension cut-off condition in the principal stress space. When the combination of principal stresses violates this condition, the crack is initiated. In the present study attention is confined to only one strength parameter, viz. the uniaxial tensile strength f_{ct}, involving the tension cut-off to reduce to a maximum stress condition. When tensile cracking is not accompanied by significant lateral compression this postulate is justified (Kupfer et al. 1969). Upon initiation, the crack is assumed to be oriented perpendicular to the direction of the major principal tensile stress, which is accepted and correct in the absence of significant lateral compression.

Less agreement has settled over the years as to the existence of a proper set of parameters controlling fracture propagation. One might confine himself to the single strength parameter and assume a sudden stress-drop upon fracture initiation. However, these strength criteria have been criticized for they suffer from non-objectiveness. Other attempts aimed at extending the principles of linear elastic fracture mechanics and elastic-plastic fracture mechanics to cementitious materials, but were judged to be inadequate either since the pursuit of unique critical stress-intensity factors, J-integrals and R-curves largely remained without success.

To date, the most versatile alternative in finite element analysis is to use a mode I fracture function that embodies tensile softening (Hillerborg et al. 1976, Bazant and Oh 1983). The parameters are the fracture energy G_f, which is defined as the amount of energy required to create one unit of area of a mode I crack, and the shape of the tensile-softening diagram. These two parameters are assumed to be fixed material properties. With respect to G_f this postulate is justified since experimental data show that the energy required to fracture mode I specimens is fairly proportional to the surface area generated. Typical values lie in the range between 50 and 200 J/m^2, depending on concrete quality.

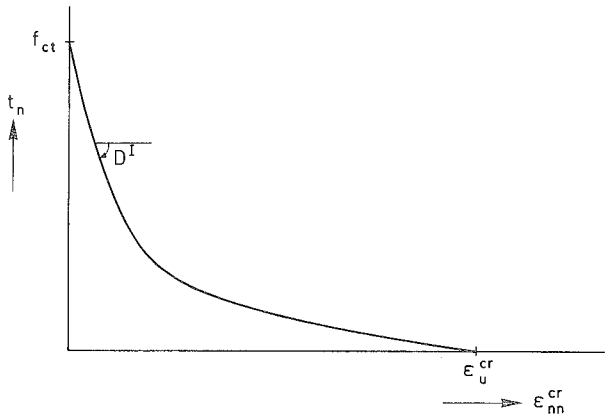

Fig. 3.1. Nonlinear mode I tensile softening relation between crack normal traction and crack normal strain (Reinhardt et al. 1986).

There is no consensus on the question whether the tensile-softening diagram is a material property. Although experimental results show uniformity in their identification of a concave curve with a steep decline just after the peak, the softening diagrams employed currently vary from linear and bilinear to several types of non-linear diagrams. We will mainly employ the nonlinear, exponential diagram proposed by Reinhardt et al. (1986) (Fig. 3.1). A justification thereof has been given by combined experimental/numerical work on direct tension (Rots et al. 1987, Hordijk and Reinhardt 1988).

Finally, the crack stiffness moduli must be expressed in terms of the strength parameter, the energy parameter and the shape of the softening diagram. For a fixed single crack the definition of G_f gives

$$G_f = \int t_n^{cr}\, du_n^{cr} \tag{3.3}$$

which corresponds to the area under the softening curve for a discrete crack. Here, t_n^{cr} is the crack normal traction and u_n^{cr} is the crack normal displacement. Evaluation of (3.3) simply results in a tangential softening modulus for a single discrete crack

$$C^I = -\frac{1}{k}\frac{f_{ct}^2}{G_f} \tag{3.4}$$

with k reflecting the shape of the softening diagram (k=2 for linear softening and k=0.74 for the initial slope of the nonlinear softening diagram of Fig. 3.1).

For smeared cracks, the fracture is distributed over a crack band width h, which is related to the particular finite element configuration. Consequently, the energy should

be released over this width in order to obtain results that are objective with regard to mesh refinement (Bazant and Oh 1983). Assuming a constant strain distribution over the crack band gives $u_n^{cr}=h\varepsilon_{nn}^{cr}$. This leads to

$$D^I = -\frac{1}{k}\frac{f_{ct}^2 h}{G_f} \tag{3.5}$$

The assumption of constant crack strain over the crack band is justified for lower order elements and for particular cases of symmetry. It does not hold for higher order elements, but the error introduced is offset by different aspects, such as the necessity to specify the crack band width a priori and the problem of definition in case of zig-zag bands. In this study h has been estimated according to the suggestions by Rots (1988). Basically, the uncertainties arise from the fact that the introduction of h into D^I constitutes only a first step towards a non-local softening model. Mathematically consistent types of non-local models that incorporate the micro-structure of continua are currently being pursued (e.g. Bazant 1986).

The stress-free strain ε_u^{cr} at softening completion (Fig. 3.1) is not conceived as a separate material property. ε_u^{cr} is a consequence of the crack band width h and the three properties in the model (tensile strength, fracture energy and softening diagram).

3.1.3 Mode II parameters

With the discrete crack applications in this thesis, both the shear traction and the shear stiffness after cracking have been set equal to zero. This is justified because these applications focus on pure mode I cracking, i.e. the potential discrete crack elements will be pre-aligned with the expected orientation of the principal tensile stresses. Shear tractions then only result from the inability to align the discrete elements with the principal tensile stresses exactly. Consequently, the shear tractions at the onset of cracking will be insignificant, which justifies setting them to zero. The stress rotations occur in the elastic elements at either side of the discrete crack elements.

For smeared cracks, the crack shear modulus D^{II} has in the past been assigned a constant value, which corresponds to a linear ascending relation between shear stress and shear strain across the crack. Apart from the arbitrariness involved in the particular choice for this value, the approach suffers from the drawback that the shear stress can increase indefinitely, and, hence, the principal stresses in the cracked elements rotate ceaselessly (D^{II}=0 of course constitutes an exception).

An improvement is obtained by making the shear stiffness after cracking a decreasing function of the crack normal strain (Cedolin and Dei Poli 1977, Kolmar and Mehlhorn 1984, Rots et al. 1984). The model accounts for the fact that the interlock of

aggregate particles diminishes with increasing crack opening. This phenomenon has been observed for macro-cracks and is likely to occur also when the "crack" is in the softening stage. In this study numerical experiments will be undertaken with a power law:

$$D^{II} = \frac{\left[1 - \frac{\varepsilon_{nn}^{cr}}{\varepsilon_u^{cr}}\right]^p}{1 - \left[1 - \frac{\varepsilon_{nn}^{cr}}{\varepsilon_u^{cr}}\right]^p} G \tag{3.6}$$

in which ε_{nn}^{cr} is the crack normal strain at the beginning of the load increment, ε_u^{cr} is the stress-free crack normal strain (Fig. 3.1), p is a constant and G is the elastic shear modulus. Eq. (3.6) gives a degradation of D^{II} from infinite upon initiation to zero at the stage where the softening is completed, i.e. where the micro-cracks coalesce into a macro-crack. Fig. 3.2a shows the relation for p=1. An interpretation in terms of the traditional shear retention factor is given in section 3.1.5, along with Fig. 3.2b.

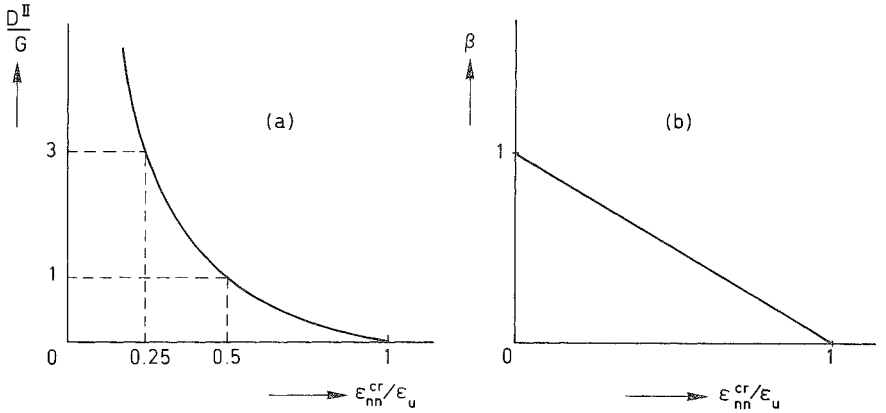

Fig. 3.2. (a) Mode II shear modulus of (3.6) which decreases with increasing crack strain. (b) The corresponding shear retention function β of (3.8).

Recalling the motives of the beginning of the chapter, (3.6) is seen as an effort towards implicit coupling between shear and normal components. The fact that (3.6) gives zero shear stiffness beyond ε_u^{cr} implies that shear stiffness from aggregate interlock across macro-cracks is ignored. This implication does not have consequences for the present study since we concentrate on the stage in which the crack comes into being and not on the confined sliding along an existing crack, or, put differently, on the stage in which the crack normal stress is tensile instead of compressive.

An advantage of (3.6) is that it is objective with respect to mesh refinement, since ε_u^{cr} is adapted to the crack band width. The traditional procedures do not meet this

requirement, with the exception of recent work by Ottosen and Dahlblom (1986).

3.1.4 Unloading and reloading

Fig. 3.3 shows the two extremes of elastic and secant type of unloading/reloading options. For elastic unloading, the crack closes immediately upon a strain reversal, whereafter further strain-decomposition is terminated and a rigorous return is made to elastic behavior. Strictly speaking, the term closing does not apply since the crack strain is irreversible. It is more correctly to speak of an inactive crack or an arrested crack. For secant unloading, the crack normal strain is reversible and upon reaching the origin of the diagram the crack truly closes, i.e. $\varepsilon_{nn}^{cr}=0$, whereafter elastic behavior is recovered.

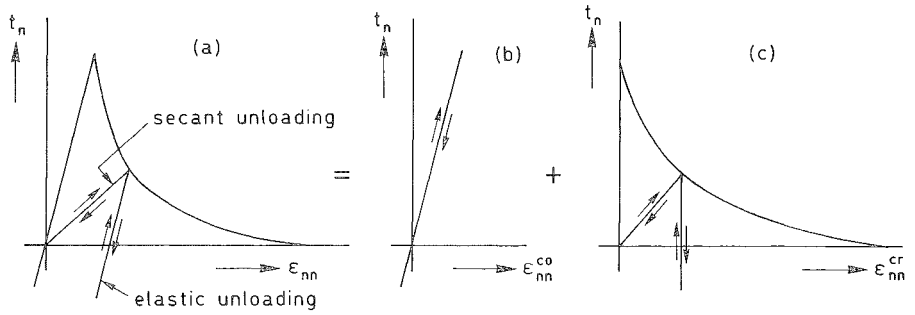

Fig. 3.3. Secant and elastic unloading in mode I elastic-softening model.
Normal stress versus total strain (a), concrete strain (b) and crack strain (c).

Neither of the two extremes constitutes an accurate approximation of reality, since cyclic tests reveal hysteresis (Reinhardt et al. 1986) The present study does not consider cyclic or non-proportional loading, but it employs the procedures for capturing non-proportional straining involved in fracture localization. In the latter case, it is of more importance *that* we distinguish between active cracks and arrested cracks than *how* we distinguish between them. For that purpose, the two extremes serve as a useful tool.

An advantage of elastic unloading is that the pre-transition part of the incremental strain at "closing", as introduced in (2.16), disappears, which keeps the computer code robust. Furthermore, since the crack "closes" abruptly, it no longer contributes to D^{crco}, which saves computational costs. Secant unloading is less attractive from this point of view. On the other hand, secant unloading somewhat accounts for the decrease of compliance with increasing crack opening strain (Reinhardt et al. 1986), whereas

elastic unloading always provides the same unloading stiffness E, even beyond ε_u^{cr}. The judge of these arguments depends on the type of application.

Upon closing, the stresses, crack strains as well as the orientation of the fixed single crack are stored in order to check for re-opening during a subsequent stage of the loading process. A closed crack will be assumed to re-open if the stress normal to it exceeds the stress which existed upon closing. In this way, re-opening is a stress-controlled process, similar to crack initiation.

A further key-aspect is that unloading and reloading appear as mode I dominated processes. The mode II behavior is assumed to be independent of the mode I status, so that it is possible for a crack to be active in mode I and inactive in mode II, inactive in mode I and active in mode II, active in both modes, or inactive in both modes. The precise handling of all state combinations is a delicate matter, not only because the crack shear strain need not vanish upon closing but also because the crack shear stress upon mode I re-opening may well differ from the crack shear stress which existed upon closing owing to stress rotations during the closed state. A proper and numerically stable procedure has been detailed in a separate paper (Rots and de Borst 1987).

3.1.5 Relation with traditional parameters

It is recalled from section 2.2.1 that traditional smeared crack formulations represent the overall shear stiffness of a cracked solid in terms of the shear retention factor β which reduces the elastic shear modulus G to βG upon cracking. β can be related to the crack shear modulus D^{II} of the present model by considering that the stiffness βG is associated with the total strain, and that D^{II} is solely associated with the crack strain. By virtue of the strain decomposition of (2.4) concrete and crack act like springs connected in series, so that the following stiffness relation holds

$$\frac{1}{\beta G} = \frac{1}{G} + \frac{1}{D^{II}} \qquad \rightarrow \qquad D^{II} = \frac{\beta}{1-\beta} G \tag{3.7}$$

in case of elastic-cracked behavior. In this way, the classical shear retention factor is re-interpreted in the spirit of mode II crack shear. For instance, the power function of (3.6) can be rewritten as

$$\beta = \left[1 - \frac{\varepsilon_{nn}^{cr}}{\varepsilon_u^{cr}} \right]^p \tag{3.8}$$

and we observe that the degradation of D^{II} from infinite (full interlock) to zero corresponds to a degradation of β from 1 (full retainment of elastic shear) to zero. Fig. 3.2

shows the functions for p=1.

Along similar lines, the series arrangement provides us with a connection between the mode I softening modulus D^I and the overall (negative) stiffness μE of the elastic softening continuum, as introduced in section 2.2.1,

$$\frac{1}{\mu E} = \frac{1}{E} + \frac{1}{D^I} \qquad \rightarrow \qquad D^I = \frac{\mu}{1-\mu} E \tag{3.9}$$

Eq. (3.9) sheds light on the condition of snap-back instability at local integration point level. We observe that μE becomes infinite or, put differently, the softening diagram reduces to a sudden stress-drop if

$$D^I = -E \tag{3.10}$$

Together with (3.5) this yields a maximum crack band width below which the softening maintains a negative slope (Bazant and Oh 1983),

$$h \leq k \frac{G_f E}{f_{ct}^2} \tag{3.11}$$

where k again reflects the shape of the softening diagram (see Eq. 3.4), which is critical at the peak if the curve is concave. If the crack band width exceeds this limit, the local stress-strain relation shows a snap-back (Carpinteri et al. 1986, Crisfield 1986, Rokugo et al. 1986) and the condition of invariant fracture energy is no longer satisfied unless we resort to reduction of the strength limit in combination with a sudden stress drop (Bazant and Oh 1983). Indeed, in the present study the strength limit has been automatically reduced once (3.11) was violated. For very large size parameters the behavior even becomes that brittle that the results approach those from linear-elastic fracture mechanics.

The above parallels with the traditional smeared crack formulation can be drawn even further, since the orthotropic law of (2.3) can be demonstrated to be a special case of the strain-decomposition approach. To this end, we elaborate (2.15) in the crack coordinate system, so that for a 2D-configuration N reads

$$N = \begin{bmatrix} 1 & 0 \\ 0 & 0 \\ 0 & 1 \end{bmatrix} \tag{3.12}$$

According to Hooke's law we have for the elastic concrete

$$D^{co} = \frac{E}{1-\nu^2}\begin{bmatrix} 1 & \nu & 0 \\ \nu & 1 & 0 \\ 0 & 0 & \frac{1-\nu}{2} \end{bmatrix} \tag{3.13}$$

Furthermore, according to (3.2), (3.7) and (3.9) the crack constitutive matrix reads

$$D^{cr} = \begin{bmatrix} \frac{\mu}{1-\mu}E & 0 \\ 0 & \frac{\beta}{1-\beta}G \end{bmatrix} \tag{3.14}$$

where $G=E/2(1+\nu)$. Substituting the above expressions for $\boldsymbol{N}$, D^{co} and D^{cr} into (2.15) yields an overall stress-strain relation which matches the orthotropic law of (2.6) (Rots et al. 1985). It is concluded that (2.3) is a special case of the strain-decomposition concept for an elastic-cracked material.

3.2 Multidirectional-crack parameters

3.2.1 Essentials

The traction-strain law for multi-directional cracks was introduced in (2.24) in the form of a constitutive matrix $\hat{D}^{cr}$ that relates the traction increment $\Delta\hat{t}^{cr}$ to the local crack strain increment $\Delta\hat{e}^{cr}$, whereby $\hat{}$ denotes an assembly. Ideally, this law should reflect interaction between the individual cracks via off-diagonal submatrices. However, the particular submatrices to be used in such an approach are not obvious, while it is not unthinkable that inclusion of them increases the level of sophistication to such an extent that it detracts from the practical usefulness of the concept. For this reason, the off-diagonal submatrices have been equated with zero. Consequently, $\hat{D}^{cr}$ reduces to a block-diagonal matrix (de Borst and Nauta 1985, Riggs and Powell 1986):

$$\hat{D}^{cr} = \begin{bmatrix} D_1^{cr} & 0 & ..... \\ 0 & D_2^{cr} & ..... \\ ..... & ..... & ..... \end{bmatrix} \tag{3.15}$$

where D_i^{cr} denotes the local stress-strain matrix for crack number i. The above arguments parallel those that led to the non-coupled format of (3.2) for a single crack.

A further assumption is that the non-coupled format for a single crack will be maintained for each multi-directional crack, i.e. each submatrix D_i^{cr} is given zero off-

diagonal terms according to (3.2). Consequently, the block-diagonal matrix reduces to a diagonal matrix.

Considering orthogonal cracks in multi-axial tension, the assumptions are justified since the state of a crack does not affect the state of an orthogonal crack. For instance, the strength limit f_{ct} is attainable in all directions (Kupfer et al. 1969), while it is also plausible that the full fracture energy G_f can be consumed for each orthogonal crack. These characteristics allow each submatrix D_i^{cr} to be filled in accordance with the single-crack rules derived in the preceding section.

For non-orthogonal cracks, the situation is less obvious and the concept bears on the way in which the damage accumulated in previous cracks is transferred to the constitutive relation for the new crack. As the block-diagonal structure of $\hat{D}^{cr}$ abandons *explicit* coupling, this transfer must be provided in an *implicit* way, by assuming the properties underlying submatrix D_2^{cr} in (3.15) to depend on the state of crack 1. This section aims at deriving transparent expressions for such implicit coupling, which is an extension to the pioneering study by de Borst and Nauta (1985) who isolated the material law for a certain crack from the state of previous cracks.

3.2.2 Some simplifications

The use of a non-zero shear retention factor for fixed cracks implies that the axes of principal stress rotate after crack formation. The inclined principal tensile stress may well increase although the fixed crack correctly shows softening, and it must be decided whether or not a subsequent crack is initiated. To this end, four criteria can be distinguished:

(a) the inclined principal tensile stress σ_1 again violates the maximum stress condition, i.e. $\sigma_1=f_{ct}$,
(b) the inclination angle between the principal tensile stress and the existing crack(s) exceeds the value of a threshold angle α,
(c) both condition (a) as well as (b) are violated,
(d) either condition (a) or (b) is violated.

Although condition (a) correctly limits the maximum tensile stress, it does not limit the total number of cracks. For high values of β (e.g. β=0.5) it is imaginable that a new crack must be initiated in almost each stage of the loading process, which becomes inefficient when permanent memory is retained. The threshold-angle condition (b) obviates this deficiency, but, conversely, does not keep control of the maximum tensile stress, especially for high values of α (e.g. $\alpha=60^o$). The same argument holds for condition (c), which was exemplified by a case whereby the principal tensile stress temporarily amounted to three times the tensile strength while the threshold angle condition

was still not violated (Rots 1985).

To clarify this issue we need further simplifications in addition to the assumption that $\hat{D}^{cr}$ is diagonal. A first simplification is achieved by adopting elastic unloading for inactive cracks (Fig. 3.3). As explained in section 3.1.4, this option excludes inactive defects from being incorporated in $\hat{D}^{crco}$. This is attractive because experimental data reveal that only the most recently initiated defect of a system of non-orthogonal defects is active, while previous defects have become inactive (Vecchio and Collins 1986, Bhide and Collins 1987). Using the elastic unloading option, it becomes feasible to consider a large number of (inactive) cracks, or, put differently, to keep the threshold angle low. Assuming that all previous cracks indeed unload, the elastic unloading option implies that the block diagonal matrix $\hat{D}^{cr}$ reduces to the single-crack matrix of (3.2) for the most recently initiated defect, which in the sequel will be referred to as the *currently-active crack*.

Once a defect has become inactive, the only motive for keeping memory of its direction is to check for re-activation during a subsequent stage of the loading process. For low values of the threshold angle this approach becomes impracticable. As an alternative to re-activating an existing defect, one may decide to activate a new defect. In doing so, defect orientations can be erased from memory altogether, which provides a second simplification. As a compromise between computational costs and degree of sophistication, the threshold angle below which memory of defect orientations has been omitted was put to 30 degrees in the current implementation. For a 2D-configuration this corresponds to a maximum storage of 6 fixed cracks.

3.2.3 Implicit coupling between non-orthogonal cracks

With the above two simplifications the identification of a proper set of multi-directional crack parameters that determine the traction-strain matrix (3.2) for the currently-active crack, becomes feasible.

The simplifications enable us to adopt the most tight condition of crack initiation, that is condition (d) of section 3.2.2, which maintains both stress control as well as orientation control. If the crack is "stress-critical", that is if it arises due to a violation of the maximum stress condition, its initial traction f_0 equals the tensile strength f_{ct}. If the crack is "threshold-critical", that is if it arises due to a violation of the threshold angle condition, f_0 is lower than f_{ct}, as indicated in Fig. 3.4. In the latter case, f_0 no longer occurs as an explicit parameter, but it is dictated by the threshold-angle condition.

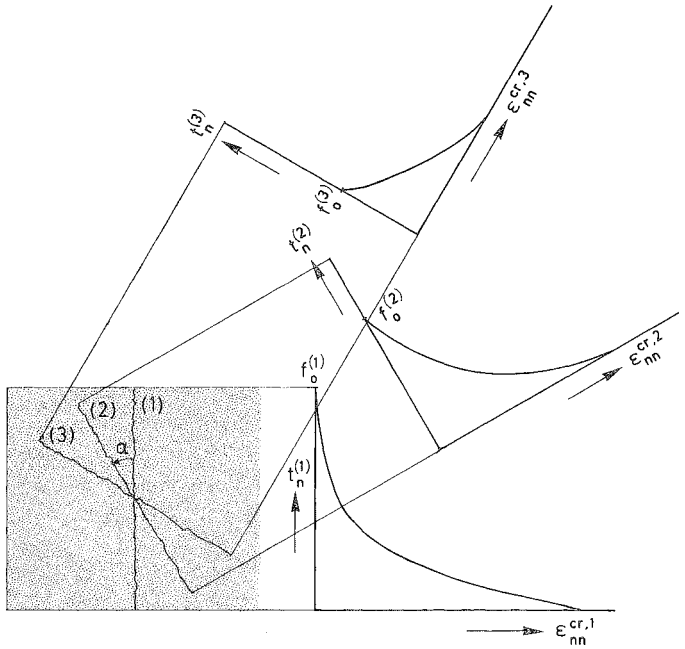

Fig. 3.4. Memory transfer in mode I softening for multi-directional cracks.
The available energy and the peak stress decrease with increasing crack number.

The fracture energy consumed in previous defects is subtracted from the energy available for the currently-active defect. The energy g_f consumed in a system of n inactive defects reads

$$g_f = h \sum_{i=1}^{i=n} \int_0^{\varepsilon_{nn}^{cl,i}} t_n^i \, d\varepsilon_{nn}^{cr,i} \tag{3.16}$$

where $\varepsilon_{nn}^{cr,i}$ is the normal strain of crack i, $\varepsilon_{nn}^{cl,i}$ is the normal strain of crack i at closing, t_n^i is the normal traction of crack i and h is the crack band width which is assumed to be the same for all cracks. The energy available for crack $n+1$ is then assumed to be $(G_f - g_f)$. This procedure, which is illustrated in Fig. 3.4, does not relate the fracture energy to a particular orientation, i.e. G_f is not conceived to be a vector as previously suggested (de Borst 1986). When full memory is retained, (3.16) can be readily evaluated since tractions and strains for all cracks, including arrested ones, are permanently available. When full memory is omitted, (3.16) must be stored and updated by adding the contribution of the preceding-active crack before making it inactive and erasing it from memory. In the latter case, the storage of (3.16) serves as "overall memory" of the damage accumulated in the system.

The shape of the softening diagram for subsequent cracks has been defined as the residual portion of the "mother" diagram, i.e. that portion of the initial, single crack

diagram that lies beyond f_0. This scheme is sketched in Fig. 3.4 and is essential with concave-shaped softening. When each subsequent crack would be assigned the same diagram as the first crack, the softening would always start with a steep slope. Such would be incorrect because it prevents the tail of the concave diagram from being effectuated.

In a previous study the shear stiffness across active cracks as well as inactive cracks was reduced, resulting in a rapid decrease of the overall shear capacity of the multiply-cracked system (de Borst and Nauta 1985). Adopting elastic unloading, only the shear stiffness across the active crack is reduced, while across the inactive cracks elastic shear capacity is re-inserted. In this case, application of a constant shear retention factor β, or, equivalently, a constant crack shear modulus D^{II}, would not account for the damage accumulated via previous cracks. It is more correctly to assume β for the currently-active crack to be a function of the crack history. To this end, the crack strain accumulated in inactive defects is recorded:

$$\boldsymbol{\varepsilon}^{cr,inactive} = \sum_{i=1}^{i=n} N_i \boldsymbol{e}_i^{cr} \tag{3.17}$$

where n is the number of inactive defects. From this vector, we calculate the principal tensile crack strain ε_{11}^{cr}, which serves as an overall damage indicator, like g_f of (3.16). Following the procedure for a fixed single crack the shear retention factor for the currently-active crack is made a decreasing function of ε_{11}^{cr}. For instance, the multiple crack analogy of (3.8) becomes

$$\beta = \left[1 - \frac{\varepsilon_{11}^{cr}}{\varepsilon_u^{cr}} \right]^p \tag{3.18}$$

where ε_{11}^{cr} replaces ε_{nn}^{cr}. When ε_{11}^{cr} exceeds ε_u^{cr}, the shear retention factor of (3.18) vanishes and the principal stress ceases to rotate. This scheme implies the crack to be truly fixed upon mode I softening completion, i.e. upon the stage where the micro-cracks coalesce into a continuous macro-crack. The subtle difference with a single crack lies in the fact that the shear stress across the latest multiple crack is only small, while the shear stress accumulated across a single crack may be significant.

3.3 Rotating-crack parameters

Having constructed constitutive relations for multi-directional cracks, the step towards the coaxial rotating crack concept as the limit of the fixed multi-directional concept becomes straightforward. Specifically, we assume

— a zero-threshold angle, and
— rigorous elastic unloading for inactive cracks,

which leads to a situation of a continuously rotating active crack. Again, overall memory of fracture energy is preserved and the mode I relation for the currently-active crack is set up along the above lines. Essentially, this implies that the multiple-crack matrix (3.15) reduces to a single-crack matrix (3.2) with a continuously changing matrix N of orientation.

The deviation now lies in the use of a specific mode II relation for the currently-active crack. As indicated in section 2.2.5, the overall shear stiffness βG which enforces coaxiality between principal stress and strain for the 2D rotating crack concept is

$$\beta G = \frac{(\sigma_{11}-\sigma_{22})}{2(\varepsilon_{11}-\varepsilon_{22})} \tag{3.19}$$

According to (3.7) this leads to the following crack shear modulus for the currently-active crack:

$$D^{II} = \frac{(\sigma_{11}-\sigma_{22})\,G}{2(\varepsilon_{11}-\varepsilon_{22})G-(\sigma_{11}-\sigma_{22})} \tag{3.20}$$

It is recalled from section 2.2.5 that an inner iteration loop is employed to prevent drifting from the coaxiality condition as induced by finite increments of strain. In the first inner iteration the principal 1,2 indices refer to the configuration at the beginning of the load step, i.e. to the current crack axes. In subsequent inner iterations they refer to the configuration beyond the previous inner iteration.

Conditions of multi-axial tension with shear may involve multiple rotating cracks. Since coaxiality is preserved, such cracks are by definition mutually orthogonal since they follow the axes of principal strain. The memory indicators of (3.16) and (3.17) must then be stored for each rotating crack direction. By virtue of the strain-decomposition, a shear reduction for two orthogonal cracks implies βG to be given by

$$\frac{1}{\beta G} = \frac{1}{G} + 2\frac{1}{D^{II}} \tag{3.21}$$

As βG again must satisfy (3.19), the crack shear moduli D^{II} for the two orthogonal rotating cracks must be taken twice the value required for a single rotating crack in order to enforce coaxiality.

While previous defects are assumed to unload elastically, possible unloading of the current (latest) defect need not be assumed to be elastic. Unloading of the current defect occurs if the continuum with the rotating crack undergoes overall unloading. We identify such a case if the crack strain increment for the current defect is calculated to be negative. When elastic unloading is assumed, all information can then be erased from memory, except for the current principal tensile stress which is stored in order to check for initiation of a new defect during a subsequent stage. Coaxiality is automatically preserved because subsequent behavior is elastic. When secant or any other type of unloading is assumed, the defect is treated in the same manner as an active defect. Hence, the coaxiality-enforcing mode II relation must be maintained during the unloading phase, as well as during a possible re-loading or re-softening phase. The mode I softening relation is replaced by the unloading relation and the negative crack strain increment for the defect gives rise to a decrease of the overall principal crack strain ε_{11}^{cr}.

Strictly speaking, it is no longer necessary to reserve the term "rotating crack" for models that preserve coaxiality between principal stress and strain. This is because the fixed multi-directional crack concept covers a wide spectrum of stepwise-rotating non-orthogonal cracks, which also permits crack shear relations different from the one enforcing coaxiality to be employed.

4. Tension-shear model problem

In this chapter an elementary tension-shear problem will be scrutinized. The purpose is to illustrate the fundamental differences between elastic-softening analyses using fixed-single cracks, multi-directional cracks and rotating cracks.

4.1 Idealization

Reference is made to the plane-stress model problem of biaxial tension and shear depicted in Fig. 4.1. It concerns an elastic-softening continuum of unit dimensions with Young's modulus E=10000 N/mm^2, Poisson's ratio ν=0.2, tensile strength f_{ct}=1.0 N/mm^2 and a linear strain-softening diagram with an ultimate strain ε_u^{cr} which equals three times the elastic strain at peak-strength, i.e. ε_u^{cr}=0.0003, corresponding to a fracture energy G_f=0.15 J/m^2 over unit crack band width h=1.0 mm. The elastic unloading option has been adopted.

Initially, the continuum is subjected to tensile straining in the x-direction accompanied by lateral Poisson contraction in the y-direction, i.e. $\Delta\varepsilon_{xx} : \Delta\varepsilon_{yy} : \Delta\gamma_{xy} = 1 : -\nu : 0$. Immediately after cracking, a switch is made to

combined biaxial tension and shear according to $\Delta\varepsilon_{xx} : \Delta\varepsilon_{yy} : \Delta\gamma_{xy} = 0.5 : 0.75 : 1$, involving the axes of principal strain to continuously rotate after crack formation as is typical of fracture propagation in smeared finite element models. This scheme was inspired by recent work of Willam et al. (1987).

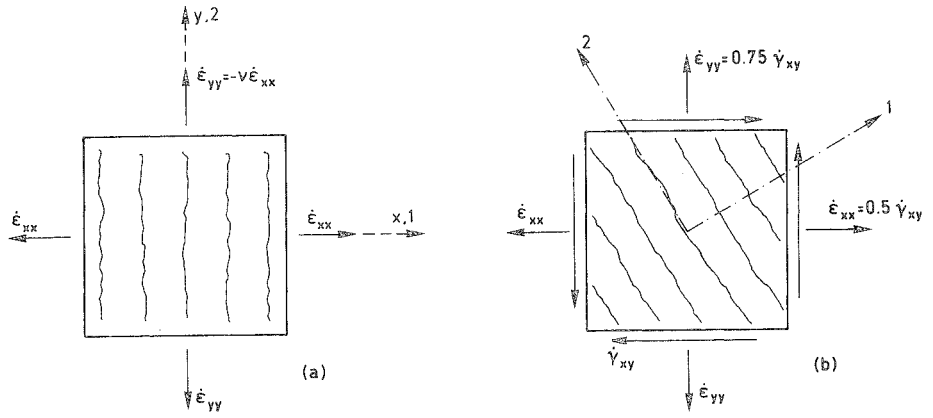

Fig. 4.1. Lay-out of tension-shear model problem.
(a) tension up to cracking; (b) biaxial tension with shear beyond cracking

Since the problem involves a homogeneous state of stress and strain, it could be idealized using a single finite element with a single Gauss-point. Standard displacement-control produced full convergence all along the softening regime.

The focus is placed on a variation of the threshold angle α, while the mode II relation across the currently-active crack is kept fixed in the form of a quadratic degradation of β with increasing principal tensile crack strain according to (3.18) with p=2. The adopted values of α range from 0, 7.5, 15, 30, 45 up to 90 degrees. The extreme of α=0^o corresponds to a continuously rotating crack (not maintaining coaxiality, however) and the other extreme of α=90^o corresponds to a fixed single-crack. In addition, the problem was analyzed using the coaxial rotating crack model, i.e. for threshold angle α=0^o and β enforcing coaxiality according to (3.19). Summarizing, the following cases have been studied:

— fixed single-crack (non-coaxial)
  threshold angle $\alpha = 90^o$
  variable shear retention factor β according to (3.18) with p=2

— multi-directional cracks (non-coaxial)
  threshold angle $\alpha = 0$, 7.5, 15, 30 and 45^o
  variable shear retention factor β according to (3.18) with p=2

— rotating cracks (coaxial)
threshold angle $\alpha = 0^o$
variable shear retention factor β according to (3.19)

4.2 Shear stress-strain response

The nominal τ_{xy}–γ_{xy} shear response is shown in Fig. 4.2. The two computations for a zero threshold angle provide the most flexible response, whereby the condition of coaxiality gives rise to an even lower maximum shear stress than the crack-strain decreasing shear retention function. In addition, these two computations show curves that are nicely smooth as a result of the continuously changing orientation of the crack. Upon increasing the threshold angle the response becomes less flexible and we observe increasing discontinuity as a result of the interval adaptation of the currently-active crack orientation to the continuous rotation of principal stress. For threshold angles beyond 45^o the initiation of inclined cracks is postponed even further and the solution approaches the fixed single-crack solution for α=90^o, which is extremely stiff.

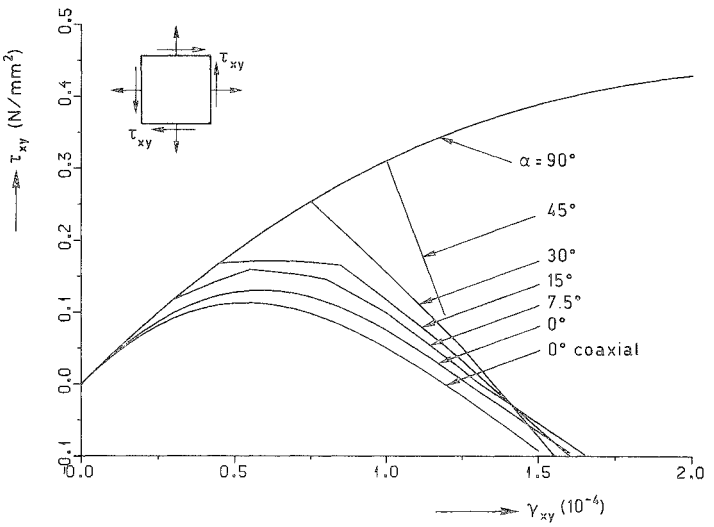

Fig. 4.2. Shear stress-strain response in x,y direction, for different threshold angles α between multi-directional cracks.

The observation of stiff behavior for fixed-single cracks corresponds to previous findings (Willam et al. 1987, Kolleger and Mehlhorn 1987, Rots and de Borst 1987, Crisfield and Wills 1989). The present results indicate that a crack-strain decreasing shear retention function does not provide a remedy. It is intriguing that the results in Fig. 4.2 for threshold angles less than 90^0 are much more flexible. These results invariably display shear softening along the x,y-plane of initial cracking. This shear softening occurs *implicitly*, as a consequence of the threshold-angle control of multi-

directional cracking and of the transfer of crack memory to the softening law for the currently-active crack.

When maintaining the concept of fixed single cracks, the unpleasant feature of stiff behavior can only be eliminated by adding *explicit* shear-softening, i.e. by prescribing a mode II shear softening diagram for the fixed plane. This was demonstrated in a previous study by Rots and de Borst (1987). In that case, however, the result is very critical to the particular shear-softening diagram adopted, which is unfortunate since experimental data to define such diagrams are lacking. The present approach with crack rotation, either stepwise or continuous, is to be preferred. The associated implicit possibility of shear softening along the x,y-plane of initial cracking is driven by the well-controlled principal stress/strain situation. The point is that it is more logical to interpret shear stress as the 'consequence' than as the 'cause' of principal stress.

4.3 Principal stress-strain response

The discrepancies further become manifest on plotting the principal tensile stress σ_{11} against the principal tensile strain ε_{11}, as shown in Fig. 4.3. Note that the directions of these identities are not aligned, except for the coaxial rotating crack result. The fixed-single crack curve (α=90°) is very illustrative as it shows σ_{11} to decrease only slightly beyond crack initiation, whereafter it re-starts to increase and amply exceeds the tensile strength. This again illustrates that the fixed-single crack concept produces stiff behavior, even when a rational shear retention function (like the present one, decreasing from 1 to zero) is employed.

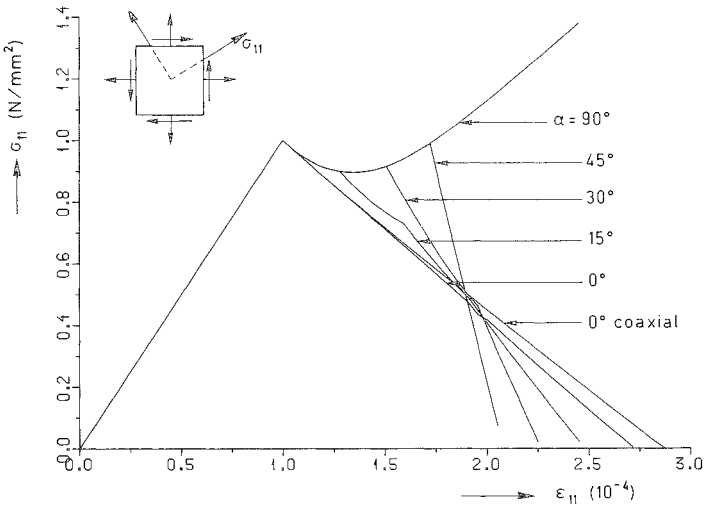

Fig. 4.3. Principal tensile stress-strain response in 1,2 direction, for different threshold angles α between multi-directional cracks.

On decreasing the threshold angle, inclined cracks arise and the tensile strength is correctly kept under control, which is reflected by the truncation of the fixed single crack curve. The curve for coaxial rotating cracks replicates the input softening diagram, which indicates that the present conception of the coaxial rotating crack concept as the limit of the fixed multi-directional crack concept correctly resembles the approach of rotating principal stress-strain relations whereby the softening is monitored explicitly in the principal axes. (Note that with the coaxial rotating crack concept the ultimate *total* strain computed ε_{11}^{tot}=0.000288 shows a slight deviation from the input value of the ultimate *crack* strain ε_u^{cr}=0.0003. This curiosity arises from the fact that the *concrete* strain ε_{11}^{co} normal to the rotating crack obviously has become slightly negative, which is due to the fact that Poisson's effect is fully retained after cracking.)

Fig. 4.4 compares the rotation of principal stress to the prescribed rotation of principal strain. Only for the coaxial rotating crack concept the axes of principal stress and strain coincide, while for all other computations the principal stress rotates much quicker than the principal strain. The fixed single-crack result provides the extreme.

It is illustrative to a posteriori extract the equivalent shear retention function from the output for the coaxial rotating crack result, i.e. the development of the $(\sigma_{11}-\sigma_{22})/2(\varepsilon_{11}-\varepsilon_{22})$ history with increasing straining. The result is shown in Fig. 4.5 and indicates β not only to rapidly decrease, but even to become negative, which explains the flexible response predicted. It underlines that the shear softening occurs implicitly as a result of the principal stress and strain situation.

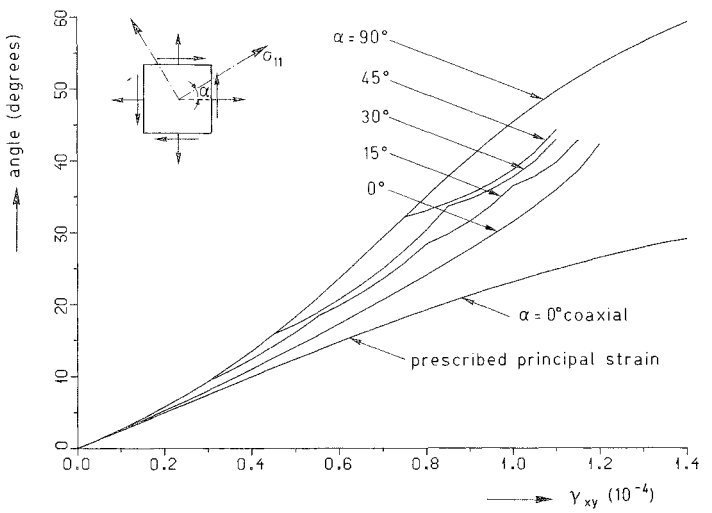

Fig. 4.4. Rotation of principal tensile stress axis, for different threshold angles α between multi-directional cracks.

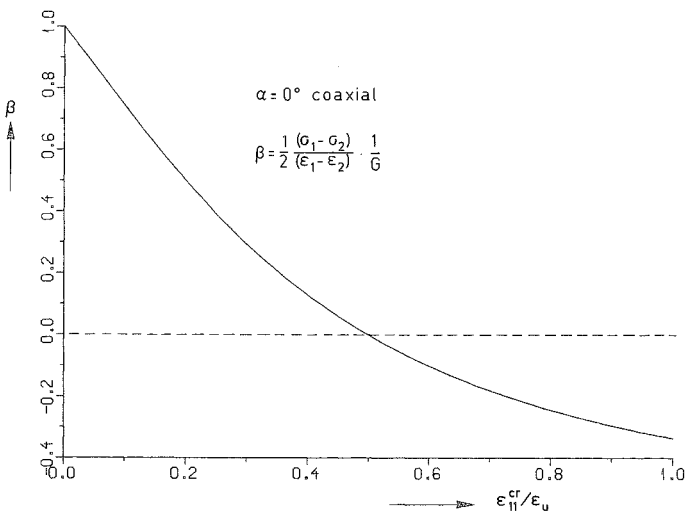

Fig. 4.5. Development of equivalent shear retention factor β for coaxial rotating crack result (extracted a posteriori according to Eq. 3.19).

4.4 Further results

The associated σ_{xx}–ε_{xx} response normal to the plane of initial cracking is shown in Fig. 4.6. Here, the fixed-single crack result instead of the coaxial rotating crack result replicates the input softening diagram since it monitors the softening explicitly in the fixed crack axes whereby the shear component does not affect the normal component because of zero off-diagonal terms in $\mathcal{D}^{cr}$. (Again, a slight deviation between ultimate total strain and input ultimate crack strain is found, for reasons described before.)

For threshold angles less than 90^o shear-normal coupling occurs implicitly due to inclined cracking, which results in a rapid degradation of σ_{xx} beyond peak stress. This demonstrates that crack rotation, either stepwise or continuous, offers an attractive alternative to the complicated issue of assessing direct shear-normal coupling terms for a fixed single crack. Note that fresh experimental results by van Mier and Nooru-Mohamed (1988) also point in this direction. Rather than producing sophisticated fixed-crack matrices, the experiments revealed some form of crack rotation or multi-directional cracking.

The σ_{yy}–ε_{yy} response in the lateral direction is shown in Fig. 4.7. Again, the fixed single-crack result forms an upperbound, which partially explains the observation of excessive orthogonal cracking in smeared analyses (Leibengood et al. 1986). Crack rotation, either stepwise or continuous, removes this behavior and correctly shows degradation of strength in the lateral direction.

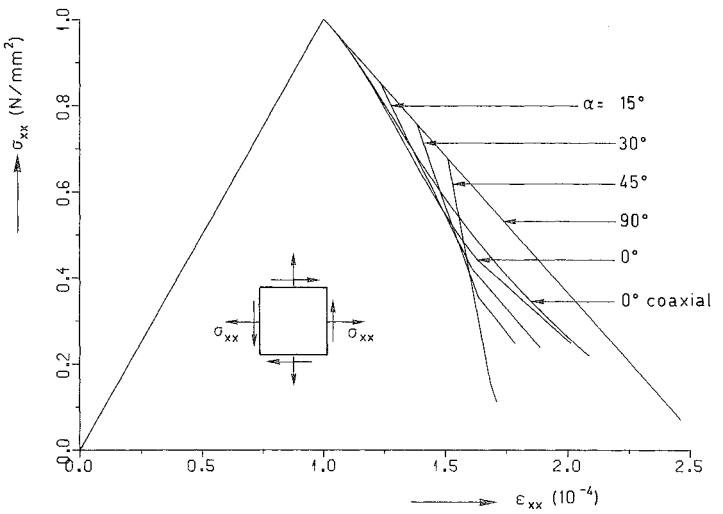

Fig. 4.6. Normal stress-strain response in x direction, for different threshold angles α between multi-directional cracks.

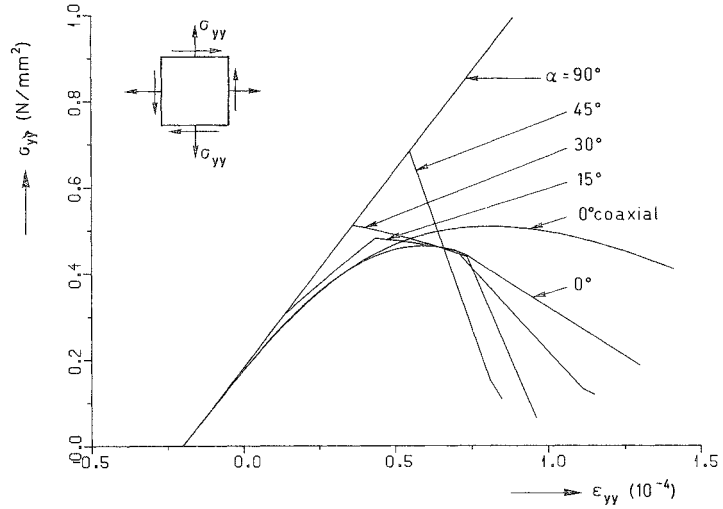

Fig. 4.7. Normal stress-strain response in y direction, for different threshold angles α between multi-directional cracks.

It is finally mentioned that from among the variety of mode II relations and threshold angles to be inserted, some additional combinations were examined. For instance, the crack-strain decreasing shear retention function was replaced by a constant shear retention factor of 0.2 or 1.0, the latter one of which induces pure mode I defects along the line of Litton's model (Litton 1974). However, these analyses suffered from lack of realism since the principal stress continued to excessively rotate, also beyond the

stage where the fracture energy was fully exhausted. Another combination investigated was the coaxiality-enforcing mode II relation of (3.19) with a non-zero threshold angle instead of a zero threshold angle. This attempt remained without success either, since the drift from the coaxiality condition could not be kept under control.

4.5 Conclusions

- The fixed-single crack concept produces stiff response, even if rational shear retention functions are employed.
- The coaxial rotating crack concept produces flexible response and keeps the maximum tensile stress under control.
- When proper transfer of damage memory is included, the fixed multi-directional crack concept provides the bridge between the two extremes of the fixed single-crack concept and the coaxial rotating crack concept.
- Crack rotation, either stepwise or continuous, implicitly provides for shear softening across the plane of initial cracking. This offers an attractive alternative to explicit shear-softening for a fixed-single crack.
- Crack rotation, either stepwise or continuous, implicitly provides for shear-normal coupling across the plane of initial cracking. This offers an attractive alternative to explicit shear-normal coupling for a fixed-single crack.

In order to prevent the reader from being overinformed, the discussions in the remaining part of this article will be confined to the two extreme cases of fixed single cracks and coaxial rotating cracks. For further results on the intermediate option of multi-directional cracks, the reader is referred to Rots (1988).

5. Tension-shear fracture problems

The present chapter extends the work of the preceding chapter to cases of localized fracture in element assemblies. Generally speaking, the lines of the fracture will deviate from the lines of the mesh, such that the fracture will propagate through the mesh in a zig-zag manner. This misalignment involves local mode II shear effects at integration point level, even if the overall fracture is of the mode I tension type. The principal stresses in the cracked elements will consequently rotate, which calls for a careful examination of the various crack concepts.

In addition to stress rotation, attention will be given to stress-locking. This phenomenon may occur whenever smeared softening laws are employed in finite element analyses. This will be demonstrated by comparing the smeared crack results with discrete crack results.

5.1 CLWL-DCB specimen

We consider a Crack-Line-Wedge-Loaded Double-Cantilever-Beam which has been tested by Kobayashi et al. (1985) (Fig. 5.1). The specimen of 50.8mm thickness is assumed to be in a state of plane stress, and is subjected to a wedge load F_1 as well as a diagonal compression load F_2. The ratio of the diagonal force to the wedge force is kept approximately constant at 0.6 until a predetermined diagonal force of 3.78 kN is reached, whereafter the diagonal force is kept constant and only the wedge force alters. The diagonal force is applied under load control and the wedge load under direct wedge opening displacement control. The loading scheme implies that the notch tip is in a state of tension-tension. The fracture propagates in mode I from the notch towards the upper-right corner (Fig. 5.1b). The finite element mesh consists of four-point integrated four-node quadrilaterals, but the use of different element types does not affect the conclusions (Rots 1988).

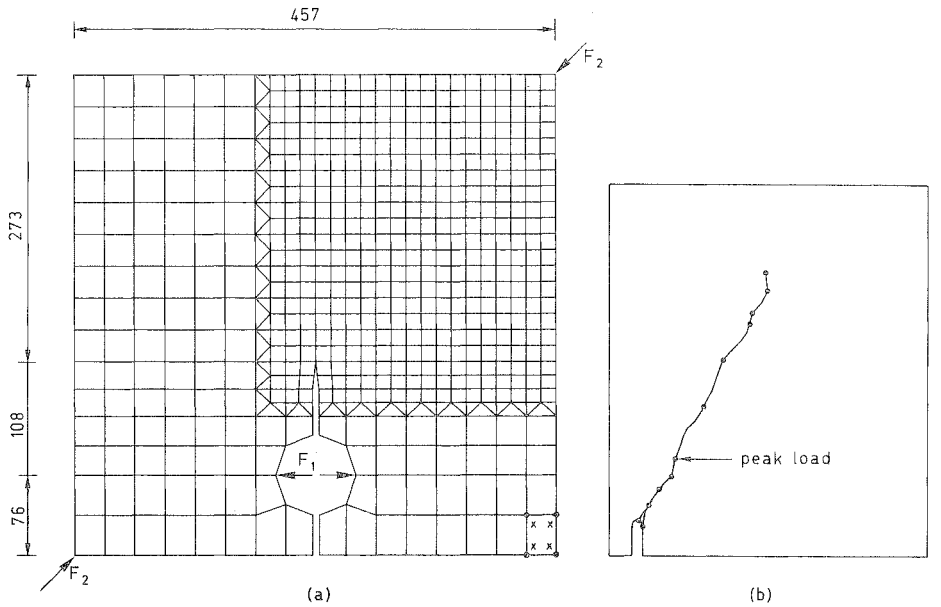

Fig. 5.1. (a) Finite element idealization of notched CLWL-DCB specimen, dimensions mm; (b) experimental results (Kobayashi et al. 1985)

A curve-fitting of the experimental result has not been undertaken, although this is no doubt possible by optimizing the mode I parameters. Rather, we will concentrate on an objective match between the smeared crack results and the discrete crack result. The elastic-softening parameters have been taken as: Young's modulus

E=30000 N/mm^2, Poisson's ratio ν=0.2, tensile strength f_{ct}=3.0 N/mm^2, fracture energy G_f=100 J/m^2 and the concave softening diagram of Fig. 3.1. The crack band width h was estimated to be $\sqrt{2}$ times the element size (Rots 1988), i.e. 14 mm.

Five computations will be compared:

— fixed smeared cracks
  α=60°, β≈0 (in fact 0.001 to avoid numerical problems)
— fixed smeared cracks
  α=60°, β=0.05
— fixed smeared cracks
  α=60°, variable β according to (3.8) with p=2
— coaxial rotating smeared cracks
  i.e. α=0, β enforcing coaxiality according to (3.19)
— predefined discrete crack
  zero shear stiffness and zero shear tractions,
  its location was adapted to the average of the smeared crack predictions.

Note that the high inclination angle α=60° in fact implies a restriction to fixed single cracks, or fixed almost-orthogonal cracks without any transfer of damage memory.

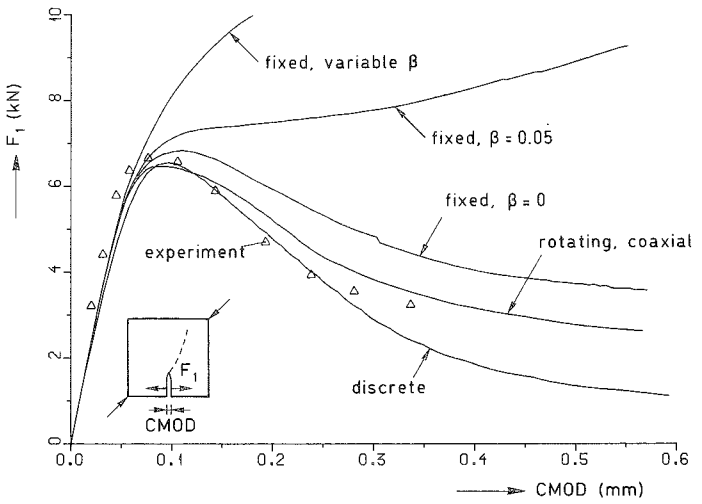

Fig. 5.2. Load-CMOD response of CLWL-DCB specimen for different crack models.

Fig. 5.2 presents the (truly converged) solutions in terms of the wedge load versus Crack Mouth Opening Displacement. We observe that all smeared crack results are too stiff in the post-peak regime. Only the rotating smeared cracks and the fixed smeared cracks with β≈0 appear capable of producing a limit point with subsequent softening.

Fixed smeared cracks with significant shear retention fail in this respect. The latter statement already holds for a β value of 0.05, which is low compared to what is commonly used in engineering practice. The result for β=0.05 shows that the limit point has vanished while the response continues to shelve instead of to soften. For the variable shear retention factor that decreases with increasing crack strain, or any other high shear retention factor, the prediction becomes even worse as we observe the response to ascend steeply, even beyond a wedge load of 10kN.

The fact that fixed cracks perform adequately only in conjunction with a zero or almost zero shear retention factor is surprising, yet explainable. Such a model in which crack shear tractions remain zero or almost-zero, implies the axes of principal stress to be fixed or practically fixed after crack formation. Stress rotation is then caused by the surrounding elastic elements, while any rebuild of principal tensile stress in the cracked elements is constrained to occur parallel to the first crack. Non-zero shear retention factors provide an additional possibility of rebuilding principal tensile stress in the cracked elements, namely via rotation in an inclined direction. Whenever such an additional opportunity of stress rebuild is given, it is eagerly utilized. This explains the overstiff responses and provides a straightforward extension to the conclusion from the model problem of the preceding chapter.

The two best possible smeared crack results are found for an almost-zero shear retention factor or the coaxiality-enforcing shear retention factor of (3.19). Here, the rebuild of stress in inclined directions does not occur and a reasonable softening response is found. Figs. 5.3 and 5.4 illustrate the fracture localization for these two cases. We observe that diagonal stretch bands through regular meshes can be predicted. On average, the effective crack band width turns out to reasonably agree with the assumed input value of $\sqrt{2}$ times the element size. With fixed cracks of almost zero shear retention the experimental direction of fracture propagation (Fig. 5.1b) is captured surprisingly well, whereas with the coaxial rotating crack concept the localization prefers to follow the lines of the mesh. This suggests that the fixed crack concept suffers less from directional bias than the coaxial rotating crack concept.

5.2 Stress-locking

Fig. 5.5 shows the genuine separation obtained for the predefined discrete crack analysis. This analysis produces the most flexible load-CMOD response and it is surprising that even the two best possible smeared crack results are significantly stiffer (Fig. 5.2). To investigate the underlying causes, the principal stresses have been plotted in Fig. 5.6 for the various computations.

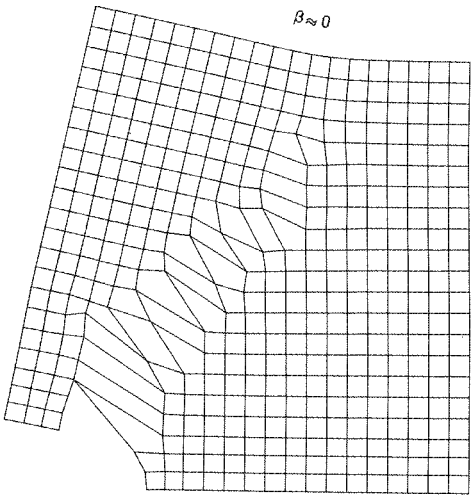

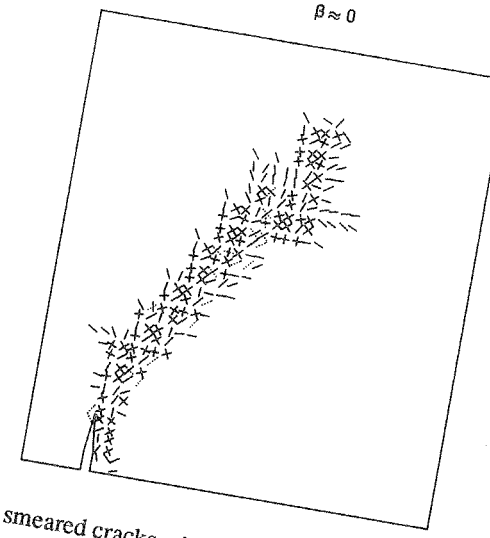

Fig. 5.3. Fracture localization for fixed smeared cracks with $\beta \approx 0$.

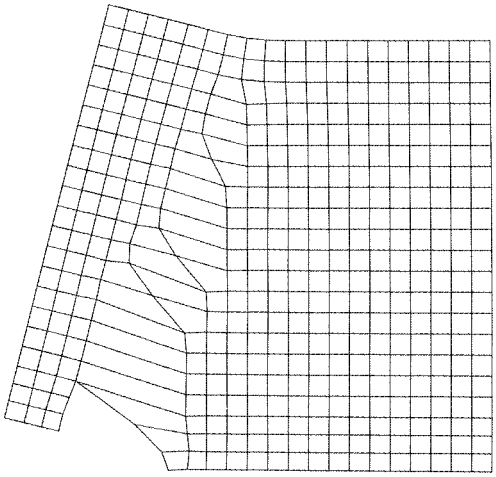

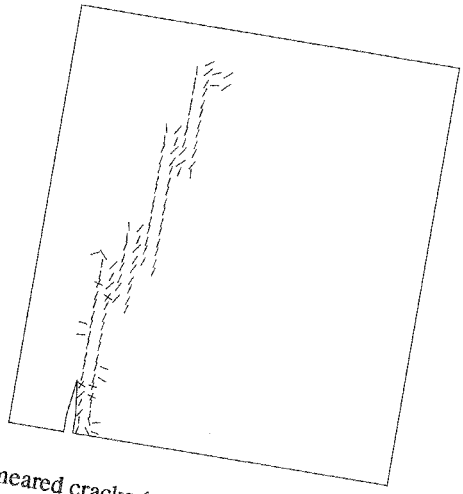

Fig. 5.4. Fracture localization for rotating smeared cracks (coaxial).

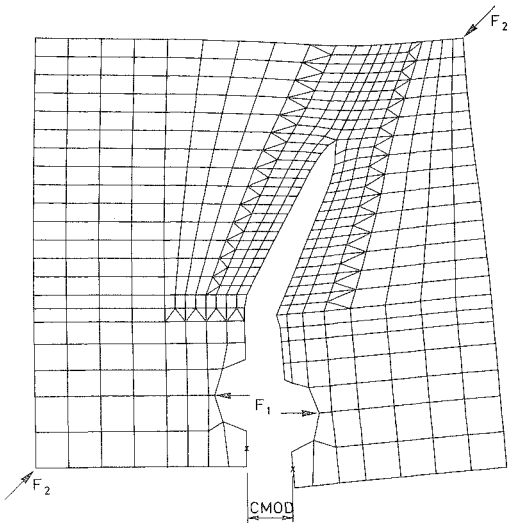

Fig. 5.5. Genuine separation for predefined discrete crack.

For fixed cracks with β=0.05 (Fig. 5.6a), we observe that the tensile stresses in the vicinity of the localization entirely refuse to decrease. Rather, the plot exhibits locked-in stresses at locations where the stress should actually drop to zero. This strengthens the explanation of overstiff response. For even higher values of β or the variable β, the plots (not shown here) became even worse and revealed very severe stress-locking. More interesting, however, is that even the two best possible, i.e. most flexible, smeared crack solutions (fixed cracks with $\beta \approx 0$ and coaxial rotating cracks) are not free from stress-locking (Figs. 5.6b and 5.6c). For both cases we observe noise in the stress profiles, especially at places where the fracture zig-zags through the mesh. It is emphasized that all solutions depicted involve truly converged equilibrium states, i.e. the curious stress patterns did *not* result from numerical inaccuracies or failure of the iterative procedure. Instead, *this stress-locking is a fundamental consequence of finite element displacement continuity in smeared softening approaches.*

If a certain element contains an inclined crack, the strain imposed by this crack implies adjacent elements to be strained as well, as illustrated in Fig. 5.7 where element 1 is subjected to tensile straining due to the inclined crack at element 2. In other words, this means that element 1 cannot be truly separated from element 2. Hence, while the stress at element 2 correctly softens, the stress at element 1, which is still in the elastic regime, increases. Then, we have two possibilities: the stress at element 1 will either exceed the tensile strength and start softening, or it will not. The former possibility is undesirable as it discourages localization (spurious cracking), but the

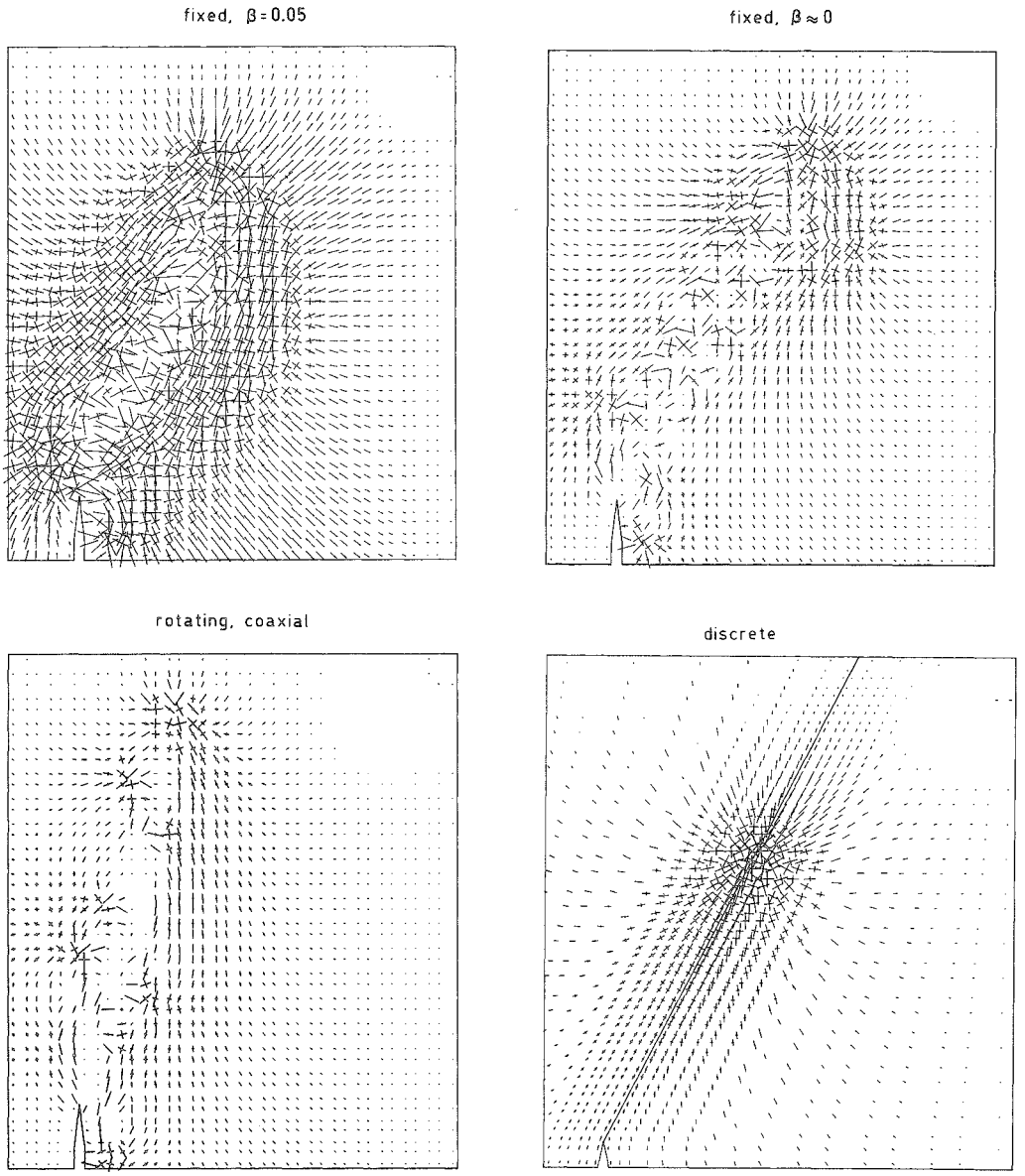

Fig. 5.6. Principal tensile stress trajectories for CLWL-DCB.
(a) severe stress locking for fixed smeared cracks with β=0.05
(b) stress locking for fixed smeared cracks with β=0
(c) stress locking for rotating smeared cracks (coaxial)
(d) correct stress relief at either side of discrete crack.

latter possibility is undesirable either, as the stress is locked-in (spurious stiffening).

The discrete crack concept starts from displacement-*in*compatibility. For the discrete crack analysis we observe that the stress plot is undisturbed and that the stresses at either side of the separation correctly come down to zero, which is in agreement with the physical process.

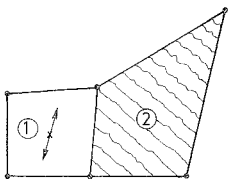

Fig. 5.7. Consequence of displacement compatibility in smeared cracking.
Strain of inclined crack at element 2 induces locked-in stress at element 1.

The above sketched behavior is obvious. Nevertheless, it has received only little attention, as far as the writer is aware of. Smeared crack results are generally presented in terms of deformed meshes and crack patterns, whereas the reader is kept without detailed resolutions of stress fields. The stress-locking is judged to be serious because:

- For different problems like reinforced beams where several localizations occur, stress-locking overstiffens the response already in the pre-peak regime.
- Stress-locking does not disappear on mesh refinement, since mesh refinement does not remove the fundamental assumption of displacement compatibility.
- Stress-locking is not exclusive for the present four-node elements, but it also occurs with different element types such as three-node, six-node and eight-node elements (Rots 1988).
- Stress-locking not only pertains to smeared cracking, but it is likely to occur whenever a smeared softening approach (also softening plasticity) is used to simulate localization.

The solution must be primarily sought in improvements of the finite element approximation. A possibility is to interactively align the elements with the lines of the fracture, or to remove fully strain-softened elements from the mesh, thus permitting adjacent elements to relax. However, with the former method the featuring advantage of smeared cracking as to maintaining the original topology is lost, and one may quite as well resort to the discrete concept. Another possibility is to use some isotropic softening law, whereby not only the stiffness normal to the crack but also the stiffness

parallel to the crack deteriorates. In the present model, this stiffness amounts to $E_{tt}=E/(1-\nu^2\mu)$, according to Eq. (2.3). Residually, this gives E when the softening is completed ($\mu=0$). With isotropic softening the residual E_{tt} becomes zero, which possibly gives more flexibility, although it must be said that such a model is not realistic since in reality the stiffness of concrete struts parallel to the cracks does not disappear.

5.3 Single-notched shear beam

To investigate the generality of the statements in the preceding section, a different problem has been investigated. It concerns a single-notched shear beam which fails in curved mode I fracture (Arrea and Ingraffea 1982). Readers who are familiar with the subject may feel disappointed since the beam has already been scrutinized (e.g. Glemberg 1984, Ingraffea and Saouma 1985, Oldenburg 1985, Rots et al. 1985, de Borst 1986, Lubliner et al. 1989). However, none of the smeared crack solutions presented so far has been able to predict full separation and softening down to zero, which calls for a renewed investigation.

The mesh is shown in Fig. 5.8 and consists of three-node triangles in cross-diagonal pattern. The steel beam ACB has not been included in the mesh. Instead, the loading has been applied at the points A and B, while controlling the notch tip opening-displacement in order to capture the snap-back involved (de Borst 1987). The parameters were taken as: E=24800N/mm^2, ν=0.18, f_{ct}=2.8N/mm^2, G_f=100J/m^2, concave softening (Fig. 3.1) and h=12mm.

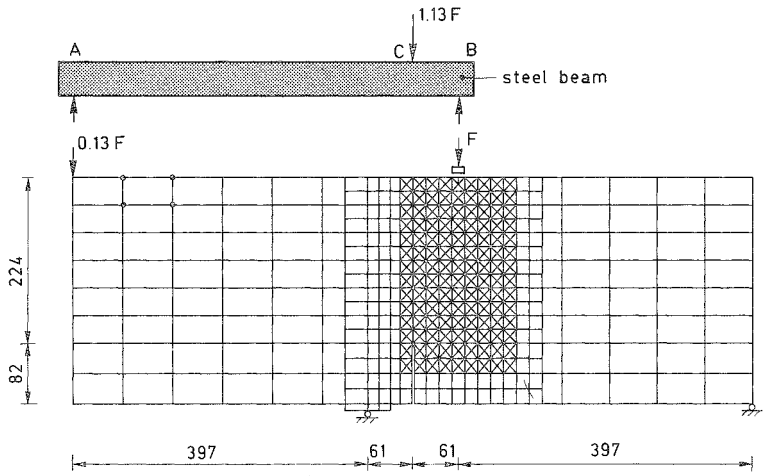

Fig. 5.8. Element mesh for smeared crack analysis of single-notched shear beam.

Five solutions are presented, corresponding to those of the CLWL-DCB specimen, i.e. fixed smeared cracks with $\beta \approx 0$, $\beta = 0.05$ and the variable β of (3.8) with $p=2$, rotating smeared cracks with the coaxiality-enforcing β of (3.19), and a predefined discrete crack with zero shear stiffness and zero shear tractions after cracking. The location of the discrete crack was predefined according to the prediction by the rotating smeared cracks. The (truly converged) solutions are summarized in Fig. 5.9, giving the load F versus the Crack Mouth Sliding Displacement, and Fig. 5.10, giving the load F versus the displacement of the master loading point C (which is recalculated from the displacements of the minor loading points A and B on the assumption that the steel beam is infinitely stiff).

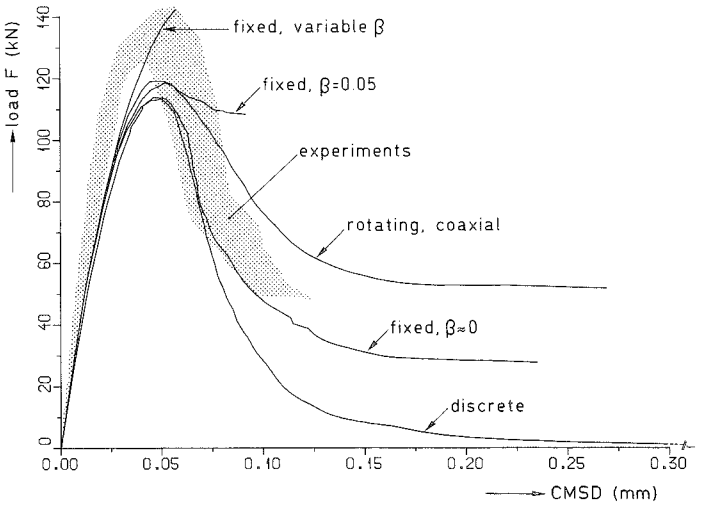

Fig. 5.9. Load F versus CMSD of single-notched shear beam of Fig. 5.8.

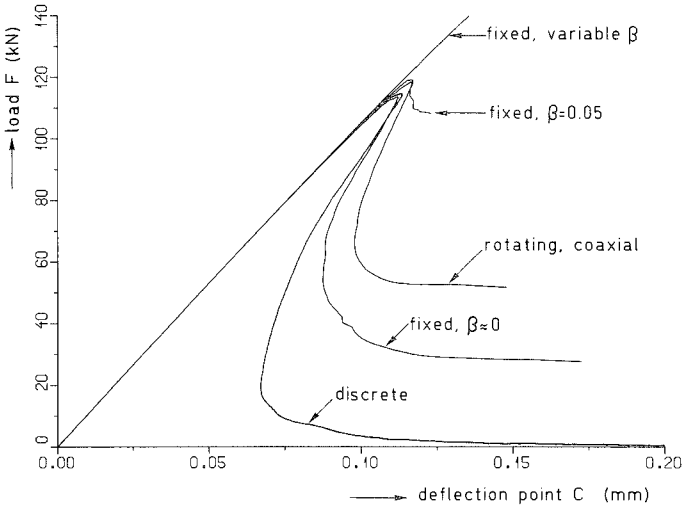

Fig. 5.10. Load F versus deflection point C of single-notched shear beam of Fig. 5.8.

Again, all smeared crack results are too stiff in the post-peak regime. Fixed cracks with $\beta \approx 0$ and coaxial rotating cracks are the only assumptions that lead to distinct softening, but the residual load plateau is incorrect. For the coaxial rotating crack result the principal stresses and the localization have been plotted in Figs. 5.11a and 5.12a. Fig. 5.11a again reveals stress-locking and spurious stiffening at either side of the localization. For fixed cracks with $\beta=0.05$ the softening ceases to proceed already at a residual load of 90 percent of the limit load. Fixed cracks with the variable β provide no softening at all. With these two computations severe stress rebuild in inclined directions was again encountered.

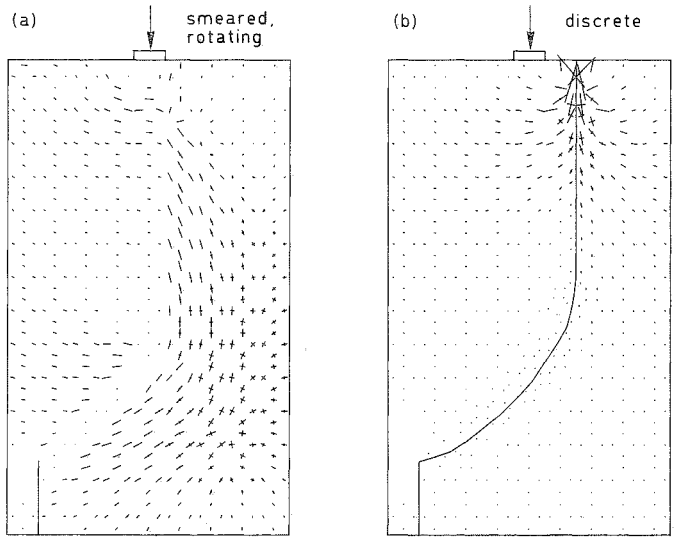

Fig. 5.11. Principal tensile stresses for single-notched shear beam at final stage.
(a) Stress-locking for smeared cracks (coaxial, rotating).
(b) Correct stress relief at either side of predefined discrete crack.

The tendency of the results is in line with the findings for the CLWL-DCB specimen. It is concluded that the phenomena have general validity. A third example that supports this assertion has been detailed separately (Rots and de Borst 1987).

With the present beam, the discrete crack solution is very illustrative since it shows softening down to zero. Fig. 5.12b reveals complete separation and the analysis does not render any locked-in stresses (Fig. 5.11b). The solution gives an excellent demonstration of the elastic-softening theory in that the energy supplied to the beam, which is represented by the integral of the master load $1.13F$ versus the master loading point displacement C in Fig. 5.10, precisely balances the fracture energy G_f times the surface area generated. With the smeared crack solutions such an interpretation is disturbed by the stress-locking.

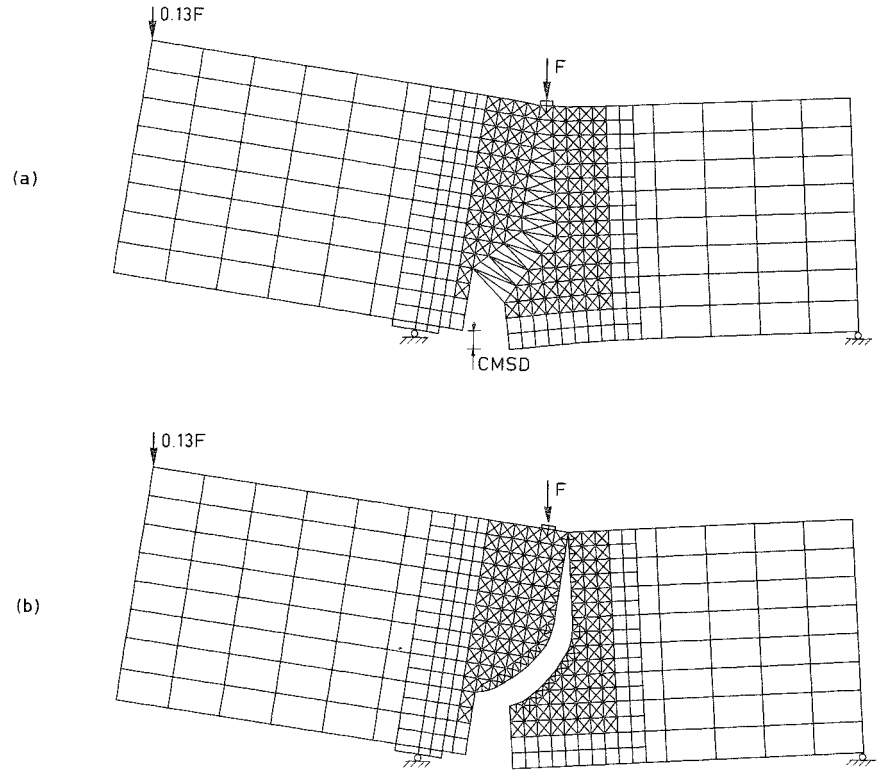

Fig. 5.12. Deformed meshes for single-notched shear beam at final stage.
(a) Localization for smeared cracks (coaxial, rotating).
(b) Genuine separation for predefined discrete crack.

From Fig. 5.9 we observe that the experimental scatter also shows a somewhat stiff behavior at the end of the softening regime. Hence, it might even be claimed that some of the smeared crack results are not too bad. However, for the experiment stiff behavior may be due to energy consumption in aggregate interlock or friction near the bearing platens, whereas for the smeared crack results stiff behavior is due to stress-locking. The agreement must therefore be regarded as a lucky coincidence since it is incorrect to claim that stress-locking constitutes a reliable representation of e.g. aggregate interlock. Rather, the present smeared crack results should have matched the ideal elastic-softening result for the mode-I conceived discrete crack.

A final comment is made on the discrepancies between the two best possible smeared crack solutions, i.e. fixed cracks with $\beta \approx 0$ and coaxial rotating cracks. Both for the present beam and for the CLWL-DCB, these discrepancies remain negligible.

Nevertheless, the coaxial rotating crack concept is to be favored over the fixed crack concept with β=0, because (a) it is less sensitive to spurious kinematic modes (Rots 1988), (b) it generally shows faster convergence, (c) it yields better stress/strain rotations at local integration point level. The single disadvantage, namely that the rotating crack concept suffers from directional bias more than the fixed crack concept, then has to be accepted.

6. Concluding remarks

In this article a variety of crack concepts has been studied for simulating localized mode I fracture in concrete. Attention has been focused on the tension-shear conditions across the crack and the consequential rotation of principal stresses and strains. These conditions arise because the lines of the fracture generally do not coincide with the lines of the mesh.

Important deficiencies of the fixed-single smeared crack concept, as formulated in e.g. a previous volume of this issue (Rots et al. 1985), have been discovered. These relate to excessive stress rotation and stress rebuild after cracking when relatively high shear retention factors are employed. These phenomena lead to solutions that are far too stiff. This was demonstrated for an elementary model problem and for two problems of localized fracture. Acceptable fixed crack results can be achieved only with an almost-zero shear retention factor.

An attractive alternative is provided by the rotating smeared crack concept. Here, proper stress/strain rotations and a flexible response emerge because of an implicit shear retention function that guarantees coaxiality between principal stress and principal strain.

A third variant of the smeared approach is the multi-directional smeared crack concept. Using rational constitutive formulations, it has been shown that this concept provides the bridge between the two extremes of fixed-single and rotating smeared cracks. However, further research is required in order to make this concept suitable for multi-purpose use.

A general deficiency of the smeared approach, either fixed, multi-directional or rotating, is the danger of stress-locking. This phenomenon arises if smeared softening laws are applied to simulate localization and is due to the fact that the geometrical *discontinuity* is approximated using the assumption of displacement *continuity*. The discrete crack concept starts from the assumption of displacement discontinuity and does not suffer from stress-locking. It leads to correct stress relief at either side of the crack.

During the 1980's, smeared crack modeling of localized fracture has undergone rapid developments. Nevertheless, stress-locking along with different, yet unsolved problems like spurious modes, directional bias, determination of the crack band width (see e.g. Rots 1988), implies that caution should be exercised in judging the predictive capability of the approach for cases of localized fracture. Pending adequate solutions to these problems, it is suggested to use the smeared approach (preferably the coaxial rotating variant or the fixed variant with almost-zero shear retention) as a qualitative predictor of the localization, whereafter a corrector analysis is made on a mesh with a predefined crack. Fig. 6.1 shows an example for a deep reinforced beam. The utility of such analyses, and also of combined smeared/discrete analyses, has furthermore been demonstrated by Rots (1988) for bond-slip problems and anchorage pull-outs, by Wang (1989) for shear fracture in reinforced beams and by Feenstra (1989) for aggregate-interlock studies. Further applications to splitting problems and laboratory tests are currently in progress.

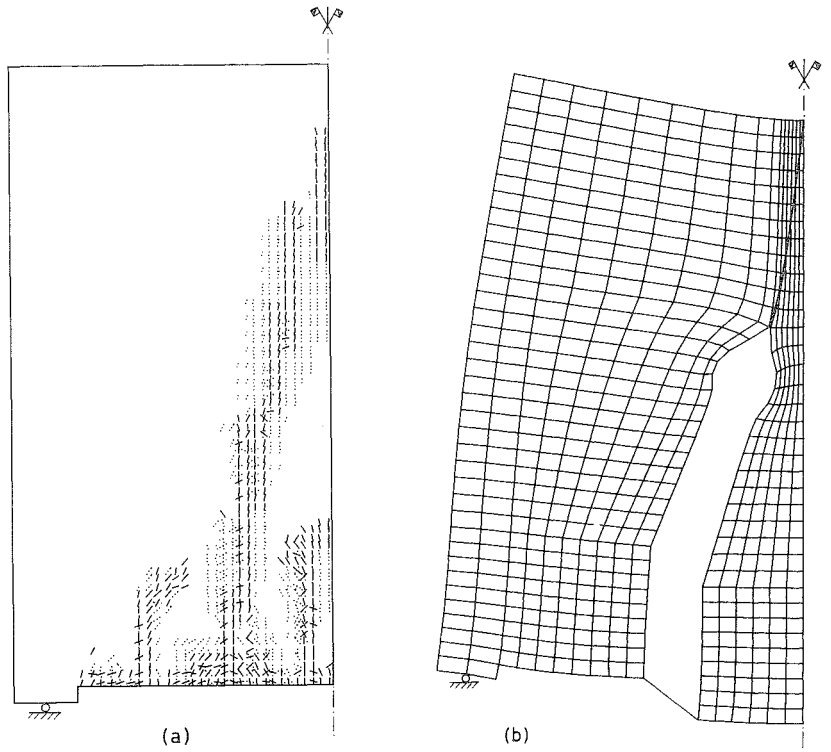

Fig. 6.1. Localized fracture in deep beam with reinforcement at the bottom side.
(a) predictor analysis with smeared cracks
(b) corrector analysis with predefined discrete crack

Acknowledgements

This publication reports on a doctoral thesis study at Delft University of Technology. The study was supported by the Netherlands Technology Foundation (STW) under grant DCT 36.0478 and by the TNO Institute for Building Materials and Structures (TNO-IBBC). The study was related to the national program on concrete mechanics, managed by the Centre for Civil Engineering Research, Codes and Specifications (CUR).

The results have been obtained using pilot-versions of the DIANA finite element program of TNO-IBBC. Support from the authors' colleague Prof. R. de Borst and from the members of the Computational Mechanics Department of TNO-IBBC supervised by Ir. G.M.A. Kusters, is gratefully acknowledged.

References

Arrea M., Ingraffea A.R., "Mixed-mode crack propagation in mortar and concrete", *Report 81-13*, Dept. Struct. Engng., Cornell Univ., Ithaca, New York (1982)

Balakrishnan S., Murray D.W., "Prediction of response of concrete beams and panels by nonlinear finite element analysis", *IABSE Reports* 54, Coll. Comp. Mech. of Reinforced Concrete, Delft Univ. Press, 393-404 (1987)

Barzegar F., "Analysis of RC membrane elements with anisotropic reinforcement", *J. Struct. Engng.*, ASCE, 115(3), 647-665 (1989)

Bazant Z.P., Gambarova P., "Rough cracks in reinforced concrete", *J. Struct. Div.*, ASCE, 106(4), 819-842 (1980)

Bazant Z.P., Oh B.H., "Crack band theory for fracture of concrete", *Materials and Structures*, RILEM, 16(93), 155-177 (1983)

Bazant Z.P., "Comment on orthotropic models for concrete and geomaterials", *J. Engng. Mech.*, ASCE, 109(3), 849-865 (1983)

Bazant Z.P., Pfeiffer P.A., "Shear fracture tests of concrete," *Materials and Structures*, RILEM, 19(110), 111-121 (1986)

Bazant Z.P., "Mechanics of distributed cracking" *Appl. Mech. Rev.*, ASME, 39(5), 675-705 (1986)

Bazant Z.P., Prat P.C., "Measurement of mode III fracture energy of concrete", *Nuclear Engng. and Design* 106, 1-8 (1988)

Bhide S.B., Collins M.P., "Reinforced concrete elements in shear and tension" *Publication 87-02*, Univ. of Toronto, Dept. of Civil Engng. (1987)

Blaauwendraad J., Grootenboer H.J., "Essentials for discrete crack analysis", *IABSE Reports* 34, Coll. Advanced Mech. of Reinforced Concrete, Delft Univ. Press, 263-272 (1981)

Blaauwendraad J., "Realisations and restrictions - Application of numerical models to concrete structures" *Finite element analysis of reinforced concrete structures*, Proc. US-Japan Seminar, (Meyer C., Okamura H. Eds.), ASCE, 557-578 (1985)

de Borst R., Nauta P., "Non-orthogonal cracks in a smeared finite element model", *Engng. Computations* 2, 35-46 (1985)

de Borst R., "Non-linear analysis of frictional materials", *Dissertation,* Delft Univ. of Techn. (1986)

de Borst R., "Smeared cracking, plasticity, creep and thermal loading - a unified approach", *Comp. Meth. Appl. Mech. Engng.* 62, 89-110 (1987)

de Borst R., "Computation of post-bifurcation and post-failure behavior of strain-softening solids", *Computers & Structures* 25(2), 211-224 (1987)

Carpinteri A., DiTomasso A., Fanelli M., "Influence of material parameters and geometry on cohesive crack propagation", *Fracture Toughness and Fracture Energy of Concrete,* F.H. Wittmann (Ed.), Elsevier Science Publ., Amsterdam, 117-135 (1986)

Cedolin L., Dei Poli S., "Finite element studies of shear-critical R/C beams", *J. Engrg. Mech. Div.,* ASCE, 103(3), 395-410 (1977)

Cervenka V., "Inelastic finite element analysis of reinforced concrete panels under in-plane loads", *Dissertation,* Univ. of Colorado, Boulder (1970)

Cope R.J., Rao P.V., Clark L.A., Norris P., "Modelling of reinforced concrete behaviour for finite element analysis of bridge slabs", *Numerical Methods for Nonlinear problems* 1, Taylor C. et al. (Eds.), Pineridge Press, Swansea, 457-470 (1980)

Crisfield M.A., Wills J., "Analysis of R/C panels using different concrete models", *J. Engrg. Mech.,* ASCE, 115(3), 578-597 (1989)

Cundall P.A., Strack O.D.L., "A discrete numerical model for granular assemblies", *Geotechnique* 29, 47-65 (1979)

Diamond S., Bentur A., "On the cracking in concrete and fibre-reinforced cements", *Application of Fracture Mechanics to Cementitious Composites,* Shah S.P. (Ed.), Martinus Nijhoff Publ., Dordrecht, 87-140 (1985)

Feenstra P.H., "Stability analysis and numerical simulation of aggregate interlock models", *Research Rep.,* Delft Univ. of Techn. / TNO Inst. for Building Mat. and Struct., to be published September (1989)

Glemberg R., "Dynamic analysis of concrete structures", *Publ. 84:1,* Dept. of Struct. Mech., Chalmers Inst. of Tech., Göteborg (1984)

Goodman R.E., Taylor R.L., Brekke T.L., "A model for the mechanics of jointed rock", *J. Soil Mech. and Foundation Div.,* ASCE, 94(3), 637-659 (1968)

Gupta A.K., Akbar H., "Cracking in reinforced concrete analysis", *J. Struct. Engng.,* 110(8), ASCE, 1735-1746 (1984)

Harmsma R.E., Nijhout J.M., "Het gedrag van betonplaten onder explosieve belastingen", *Graduate thesis,* Koninklijke Militaire Academie, Section of Civil Engng., Tilburg (1982)

Hassanzadeh M., Hillerborg A., "Concrete properties in mixed mode fracture", Proc. Int. Workshop *Fracture Toughness and Fracture Energy - Test Methods for Concrete and Rock* -, H. Mihashi et al. (Eds.), Tohoku University, Sendai, Japan, 448-451 (1988)

Hillerborg A., Modeer M., Petersson P.E., "Analysis of crack formation and crack growth in concrete by means of fracture mechanics and finite elements", *Cement and Concrete Research* 6(6), 773-782 (1976)

Hohberg J.-M., Bachmann H., "A macro joint element for nonlinear arch dam analysis", Proc. 6th Int. Conf. on *Numerical Methods in Geomechanics,* G. Swoboda Ed., Balkema Rotterdam, 829-834 (1988)

Hordijk D.A., Reinhardt H.W., "Macro-structural effects in a uniaxial tensile test on concrete", Proc. 2nd Int. Symp. on *Brittle Matrix Composites,* BMC-2, Cedzyna, Poland (1988)

Ingraffea A.R., Saouma V., "Numerical modelling of discrete crack propagation in reinforced and plain concrete", *Fracture Mechanics of Concrete*, Sih G.C., DiTomasso A. (Eds.), Martinus Nijhoff Publishers, Dordrecht, 171-225 (1985a)

Jenq Y.S., Shah S.P., "Mixed-mode fracture of concrete", *Int. J. of Fracture* (1988)

Kobayashi A.S., Hawkins M.N., Barker D.B., Liaw B.M., "Fracture process zone of concrete", *Application of Fracture Mechanics to Cementitious Composites*, Shah S.P. (Ed.), Martinus Nijhoff Publ., Dordrecht, 25-50 (1985)

Kollegger J., Mehlhorn G., "Material model for cracked reinforced concrete", *IABSE Reports* 54, Coll. Comp. Mech. of Reinforced Concrete, Delft Univ. Press, 63-74 (1987)

Kolmar W., Mehlhorn G., "Comparison of shear stiffness formulations for cracked reinforced concrete beams", *Computer-Aided Analysis and Design of Concrete Structures* 1, F. Damjanić et al. (Eds.), Pineridge Press, Swansea, 133-147 (1984)

Kupfer H., Hilsdorf H.K., Rusch H., "Behaviour of concrete under biaxial stresses", *J. Am. Concrete Inst.* 66(8), 656-666 (1969)

Leibengood L.D., Darwin D., Dodds R.H., "Parameters affecting FE analysis of concrete structures", *J. Struct. Engng.* 112(2), 326-341 (1986)

Litton R.W., "A contribution to the analysis of concrete structures under cyclic loading," *Dissertation*, Univ. of California, Berkeley (1974)

Lorig L.J., Cundall P.A., "Modeling of reinforced concrete using the distinct element method", *Proc. SEM-RILEM Int. Conf. on Fracture of Concrete and Rock*, S.P. Shah and S.E. Swartz (Eds.), SEM, Bethel, 459-471 (1987)

Lubliner J., Oliver J., Oller S., Onate E., "A plastic-damage model for concrete", *Int. J. Solids Structures* 25(3), 299-326 (1989)

van Mier J.G.M., Nooru-Mohamed M.B., "Fracture of concrete under tensile and shear-like loadings", Proc. Int. Workshop *Fracture Toughness and Fracture Energy - Test Methods for Concrete and Rock* -, H. Mihashi et al. (Eds.), Tohoku University, Sendai, Japan, 433-447 (1988)

Milford R.V., Schnobrich W.C., "Numerical model for cracked reinforced concrete", *Computer-Aided Analysis and Design of Concrete Structures* 1, F. Damjanić et al. (Eds.), Pineridge Press, Swansea, 261-273 (1984)

Ngo D., Scordelis A.C., "Finite element analysis of reinforced concrete beams", *J. Am. Concrete Inst.* 64(14), 152-163 (1967)

Nilson A.H., "Nonlinear analysis of reinforced concrete by the finite element method", *J. Am. Concrete Inst.* 65(9), 757-766 (1968)

Oldenburg M., "Finite element analysis of tensile fracturing structures", *Licentiate Thesis 1985:010L*, Lulea Univ. of Techn. (1985)

Ottosen N.S., Dahlblom O., "Smeared crack analysis using a nonlinear fracture model for concrete", *Numerical Methods for Nonlinear Problems* 3, C. Taylor et al. (Eds.), Pineridge Press, Swansea, 363-376 (1986)

Rashid Y.R., "Analysis of prestressed concrete pressure vessels", *Nuclear Engng. and Design* 7(4), 334-344 (1968)

Reinhardt H.W., Cornelissen H.A.W., Hordijk D.A., "Tensile tests and failure analysis of concrete", *J. Struct. Engng.*, ASCE, 112(11), 2462-2477 (1986)

Riggs H.R., Powell G.H., "Rough crack model for analysis of concrete", *J. Engng. Mech.*, ASCE, 112(5), 448-464 (1986)

Roelfstra P.E., Sadouki H., Wittmann F.H., "La béton numerique", *Materials & Structures* RILEM, 107, 327-335 (1985)

Rokugo K., Ohno S., Koyanagi W., "Automatic measuring system of load-displacement curves including post-failure region of concrete specimens" *Fracture Toughness and Fracture Energy of Concrete*, F.H. Wittmann (Ed.), Elsevier Science Publ., 403-411 (1986)

Rots J.G., Nauta P., Kusters G.M.A., "Variable reduction factor for the shear stiffness of cracked concrete", *Rep. BI-84-33*, Inst. TNO for Building Mat. and Struct., Delft (1984)

Rots J.G., Nauta P., Kusters G.M.A., Blaauwendraad J., "Smeared crack approach and fracture localization in concrete", *HERON* 30(1), 1-48 (1985)

Rots J.G., "Bond-slip simulations using smeared cracks and/or interface elements", *Res. Report 85-01*, Struct. Mech., Dept. of Civil Engng., Delft Univ. of Techn. (1985)

Rots J.G., "Strain-softening analysis of concrete fracture specimens", *Fracture Toughness and Fracture Energy of Concrete*, F.H. Wittmann (Ed.), Elsevier Science Publ., Amsterdam, 137-148 (1986)

Rots J.G., Hordijk D.A., de Borst R., "Numerical simulation of concrete fracture in 'direct' tension", Proc. Fourth Int. Conf. *Numerical Methods in Fracture Mechanics*, A.R. Luxmoore et al. (Eds.), Pineridge Press, Swansea, 457-471 (1987)

Rots J.G., de Borst R., "Analysis of mixed-mode fracture in concrete", *J. Engng. Mech.*, ASCE, 113(11), 1739-1758 (1987)

Rots J.G., "Computational modeling of concrete fracture", *Dissertation*, Delft Univ. of Techn. (1988)

Schnobrich W.C., Discussion of "Nonlinear stress analysis of reinforced concrete" by Valliapan S. and Doolan T.F., *J. Struct. Div.* ASCE, 98(10), 2237-2328 (1972)

Suidan M., Schnobrich W.C., "Finite element analysis of reinforced concrete," *J. Struct. Div.*, ASCE, 99(10), 2109-2122 (1973)

Tait R.B, Garret G.G., "In situ double-torsion fracture studies of cement mortar and cement paste inside a scanning electron microscope", *Cement and Concr. Res.* 16(2), 143-155 (1986)

Valliappan S., Doolan T.F., "Nonlinear stress analysis of reinforced concrete", *J. Struct. Div.*, ASCE, 98(4), 885-897 (1972)

Vecchio F.J., Collins M.P., "The modified compression-field theory for reinforced concrete elements subjected to shear", *J. Am. Concrete Inst.* 83(2), 219-231 (1986)

Walraven J.C., "Aggregate interlock: a theoretical and experimental analysis", *Dissertation*, Delft Univ. of Techn. (1980)

Wang Q.B., "Shear strength of reinforced concrete beams and slabs without shear reinforcement", *Report* 25.2.89.2.10, Delft Univ. of Techn., Faculty of Civil Engng. (1989)

Willam K., Pramono E., Sture S., "Fundamental issues of smeared crack models", *Proc. SEM-RILEM Int. Conf. on Fracture of Concrete and Rock*, S.P. Shah and S.E. Swartz (Eds.), SEM, Bethel, 192-207 (1987)